remote sensing

MDPI

Article

CARIB18: A Stable Geodetic Reference Frame for Geological Hazard Monitoring in the Caribbean Region

Guoquan Wang [1,*], Hanlin Liu [1,*], Glen S. Mattioli [2,3], Meghan M. Miller [2], Karl Feaux [2] and John Braun [4]

1 Department of Earth and Atmospheric Sciences, University of Houston, Houston, TX 77204, USA
2 UNAVCO, Inc., Boulder, CO 80301, USA; mattioli@unavco.org (G.S.M.); meghan@unavco.org (M.M.M.); kfeaux@unavco.org (K.F.)
3 Department of Earth and Environmental Sciences, University of Texas at Arlington, Arlington, TX 76019, USA
4 University Corporation for Atmospheric Research, Boulder, CO 80307, USA; braunj@ucar.edu
* Correspondence: gwang@uh.edu (G.W.); hliu30@uh.edu (H.L.)

Received: 23 February 2019; Accepted: 19 March 2019; Published: 21 March 2019

Abstract: We have developed a Stable Caribbean Reference Frame 2018 (CARIB18) using long-term continuous observations from 18 continuously operating Global Positioning System (GPS) stations fixed on the margins of the stable portion of the Caribbean plate. The frame stability of CARIB18 is approximately 0.7 mm/year in the horizontal direction and 0.9 mm/year in the vertical direction. A method that employs a total of seven parameters for transforming positional time series from a global reference frame (IGS14) to a regional reference frame is introduced. The major products from this study include the seven parameters for realizing CARIB18 coordinates and three-component site velocities of 250 continuous GPS stations (>3 years) with respect to CARIB18. Geological hazard monitoring using GPS has traditionally been performed using the carrier-phase differential method that requires single or multiple reference stations to be simultaneously operated in the field. CARIB18 allows for precise geological hazard monitoring using stand-alone GPS, which substantially reduces field costs and simplifies logistics for long-term geological hazard monitoring. Applications of CARIB18 in plate motion, post-seismic, and volcano monitoring and research are demonstrated in this article. The regional reference frame will be periodically updated every few years with more reference stations and longer periods of observations to mitigate the degradation of the frame over time and will be synchronized with the updates of the International GNSS Service (IGS) IGS reference frame.

Keywords: Caribbean; COCONET; GPS; geological hazards; monitoring; plate boundary zone; regional reference frame

1. Introduction

The Caribbean region is one of the earliest regions worldwide to employ Global Positioning System (GPS) for geological hazard studies. Due to its active tectonic and tropical environment, the Caribbean region is rife with natural hazards, such as earthquakes, volcanoes, landslides, flooding, tsunamis, hurricanes, and coastal erosions. GPS stations were installed in the Caribbean region since the middle of the 1980s for studying plate motions [1–4], almost one decade earlier than the full operation of GPS in 1995. The Caribbean region, as defined by this study, comprises the Caribbean Sea and its surrounding islands, including Central America to the west, the Greater Antilles to the north, the Lesser Antilles to the east, and parts of adjacent South America to the south (Figure 1). The tectonic entity that we refer to

as the "Caribbean plate" comprises the Caribbean Ocean Plateau and the Plate Boundary Zones (PBZs) between the Caribbean Ocean Plateau and its neighbor tectonic plates, including the North American plate to the north, the North Andes plate to the south, the South American plate to the southeast and east, and the Cocos plate and Nazca plate to the west. Figure 1 depicts the PBZs outlined based on the early concept of Caribbean PBZs proposed by Burke and Mann [5,6]. The plate boundaries are defined by Bird [7] and the GPS-derived site velocities obtained from this study. The width of PBZs varies from approximately 200 km in the western PBZ to over 600 km in the eastern PBZ. The Caribbean Ocean Plateau is often regarded as the internal and stable portion of the Caribbean plate. The PBZs surrounding the interior of the Caribbean plate are comprised of numerous microplates that have recently garnered much attention from the scientific and politico-economic communities due to the hazard risks posed to the surrounding populated island countries [8–13].

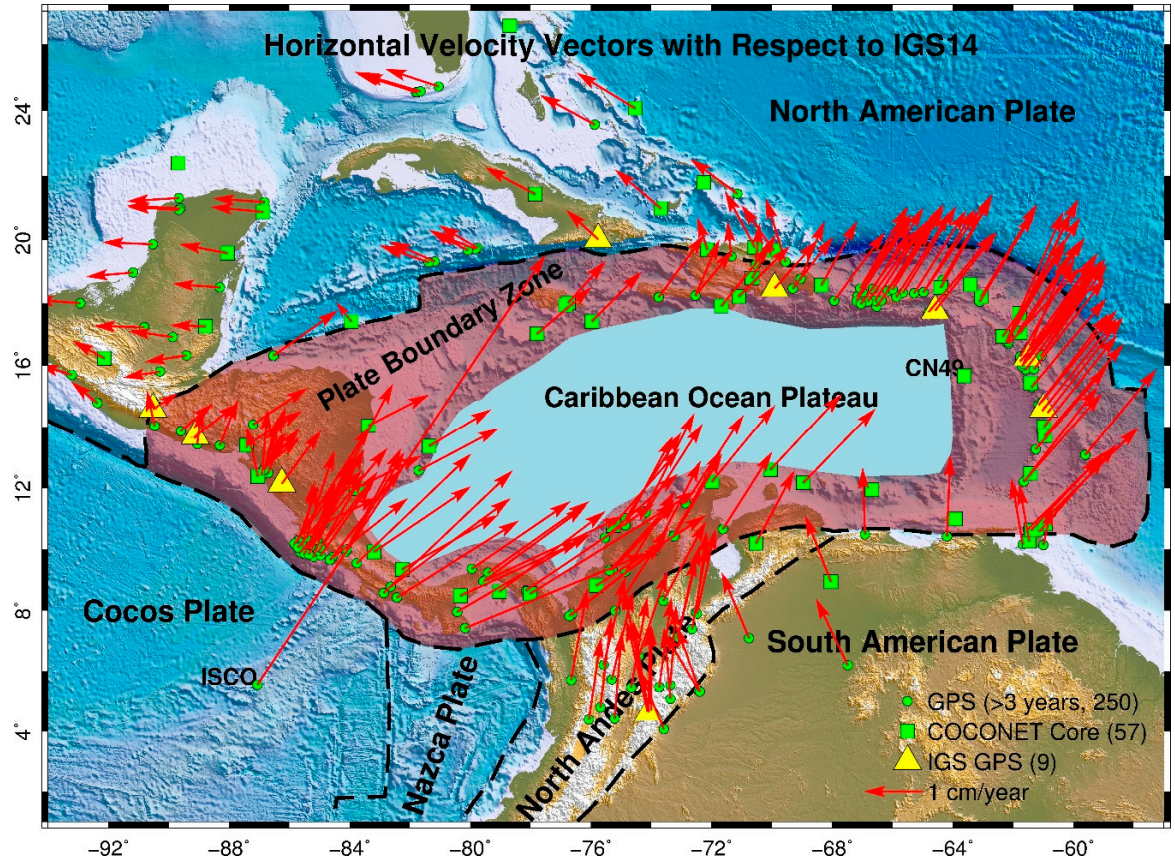

Figure 1. A map showing tectonic plates within the Caribbean region and the plate boundary zones (PBZs) between the Caribbean Ocean Plateau (the stable portion of the Caribbean plate) and its surrounding plates. The horizontal velocity vectors depict the secular plate motions at 250 permanent Global Positioning System (GPS) stations within the Caribbean region with respect to IGS14. The velocities are derived from recent GPS observations (2012–2018).

Currently, there are over 250 permanent long-term (>3 years as December of 2018) GPS stations within the Caribbean region that share raw data to the public through data archive facilities operated by UNAVCO, International Global Navigation Satellite System (GNSS) Service (IGS), Crustal Dynamics Data Information System (CDDIS) of National Aeronautics and Space Administration (NASA), National Geodetic Survey (NGS), Scripps Orbit and Permanent Array Center (SOPAC), and several other institutions. Positional time series with respect to certain regional or global reference frames are also provided by several institutions to the research community, such as the Geodesy Advancing Geosciences and EarthScope (GAGE) Facility at UNAVCO [14] and the Nevada Geodetic Laboratory

(NGL) at the University of Nevada [15]. The GPS antennas are mounted on monuments fixed on the ground or on one- to two-story concrete buildings. According to a recent investigation on closely-spaced Continuously Operating Reference Stations (CORS) in the Puerto Rico and Virgin Islands region, there is no considerable difference between building-based (one- to two-story concrete buildings) and ground-based GPS observations with regard to the precision or repeatability of daily positions and reliability of long-term site velocities as long as the buildings are stable [16]. Accordingly, we regard velocities derived from one- to two-story building-based GPS stations as free-field site velocities.

Large GPS networks in the Caribbean region include the Continuously Operating Caribbean Observational Network (COCONET, http://coconet.unavco.org), the Puerto Rico and Virgin Islands GPS network (PRVINET, http://redsismica.uprm.edu), the Nicoya Peninsula GPS Network in Costa Rica (Principal Investigator: Tim Dixon), the Sistema de Referencia Geocéntrico para las Américas (SIRGAS) Reference Network (http://www.sirgas.org), Caribbean Hurricane Prediction and Geodetic Network (PI: John Braun), Montserrat Volcano Observatory GPS Network (MVO), and other local networks. These long-term permanent GPS stations were installed by joint efforts of academic institutions, local government agencies, and land surveying companies. Unfortunately, many GPS stations within the Caribbean region were damaged by Hurricanes Irma and Maria in 2017. Some stations have not been recovered since August 2017.

The GPS dataset from a single station is not sufficient by itself to precisely measure the change of positions. GPS geological hazard monitoring projects have traditionally been conducted with a carrier-phase differential method that requires simultaneous GPS observations at rover and reference sites. Nevertheless, the instability of the reference GPS will ultimately affect the accuracy of the entire survey. Furthermore, it is not cost effective for a survey project to operate extra GPS stations outside its monitoring object, and it becomes exceedingly difficult to get ideal sites for installing reference GPS stations in urban environments. This study intends to introduce a method that utilizes stand-alone GPS for long-term geological hazard monitoring.

The need for a unified stable geodetic reference frame has become desperately urgent in the Caribbean region with the completion of the Continuously Operating Caribbean GPS Observational Network (COCONET) project along with an increasing public awareness in natural hazard monitoring using GPS. COCONET was funded by the National Science Foundation (NSF) of the U.S. in 2010 [17]. As of 2018, COCONET is comprised of 85 new and refurbished stations and over 70 existing GPS stations distributed across 26 Caribbean nations. Several COCONET stations were installed on islands sitting on the margins of the stable portion of the Caribbean plate (Figure 1). Those stations have provided fundamental datasets for realizing a stable Caribbean reference frame. This study aims to establish a stable geodetic reference frame within the Caribbean region. Publicly available GPS datasets spanning to the end of 2018 are utilized to realize the regional reference frame. Accordingly, the reference frame is called the Stable Caribbean Reference Frame 2018 (CARIB18).

2. GPS Data Processing

A complex aspect of GPS is that it initially provides positional coordinates with respect to a global reference frame, since the positions of satellites are defined with respect to a global reference frame. For high-accuracy positioning relying on post-processing, satellite ephemerides are always determined based on ground-based GPS observations from selected International GNSS Service (IGS) tracking stations. IGS08 was adopted in 2011 and then, due to the growing number of unusable stations within the IGS08 frame, was updated to IGb08 on 7 October 2012 [18]. In January 2017, IGS14 frame was adopted in parallel with the redefinition of the International Terrestrial Reference Frame 2014 (ITRF2014) [19]. The ITRF is a standard frame for referencing positions at different times and places around the world and provides the foundation for ground-based and space-based observations in Earth system sciences. IGS14 is the latest in a series of GNSS reference frames (e.g., IGS00, IGS05, IGS08) adopted by IGS [20]. In general, a global reference frame is realized with an

approach of minimizing the overall horizontal movements of a group of selected frame stations distributed worldwide. For example, the IGS08 reference stations are comprised of 232 permanent GPS stations; IGb08 reference stations are comprised of 235 permanent GPS stations [18], and IGS14 reference stations are comprised of 252 permanent GPS stations [20]. The positional coordinates for most of the GPS stations change over time with respect to global reference frames as shown in Figure 1. The site velocities with respect to a global reference frame are often dominated by the long-term drift and rotations of tectonic plates. Localized ground deformation, such as the ground motions associated with volcano activities (swelling, sinking, and cracking), fault creeping, landslides, and subsidence, could be obscured or biased by long-term plate drifts.

Accuracy and precision of GPS positioning have been improved dramatically over the past two decades due to advances in GPS hardware, software, and reference frames. The accuracy of GPS measurements (positions or displacements) does not solely rely on GPS equipment (antenna and receiver) but largely depends on how the data are collected in the field and how the data are processed [21–24]. GPS data processing algorithms generally implement two approaches: relative positioning and absolute positioning. The relative positioning approach uses simultaneous observations from two or more GPS units. One GPS unit is considered as a fixed station, also called a reference station. The relative positions are calculated using a carrier-phase differential method, which inherits high accuracy from the fact that the closely-spaced GPS units experience very similar errors and biases. The absolute positioning method determines the position of a single GPS station without using any simultaneous observations from other ground GPS stations. Precise Point Positioning (PPP) is a typical absolute positioning method [25]. The PPP method has attracted broad interests in land surface displacements and structural deformation monitoring because of its operational simplicity and consistent accuracy over time and space [26,27].

This study applied the single-receiver phase ambiguity-fixed PPP method employed by the GIPSY-OASIS (V6.4) software package, simplified as GIPSY, for calculating 24-h average (daily) positions. The GIPSY software package was developed by the Jet Propulsion Laboratory (JPL). GIPSY employs the single-receiver phase ambiguity-fixed PPP method that incorporates the Wide-Lane and Phase-Bias (WLPB) estimates from a global network of ground GPS stations to fix phase ambiguities [28]. JPL's final satellite orbit and clock products with respect to IGS14 and the WLPB estimates are used for the GIPSY processing. As of December 2018, JPL has not released its final orbit and clock products with respect to IGS14 for the years before 2002. Therefore, the GPS observations before epoch 2002.0 are not processed in this study. The other major parameters and key correction models applied during the GIPSY processing are the same as those reported in Wang et al. [29]. An outlier-detection-and-removal algorithm was applied to the positional time series derived from the PPP solutions. The details of the outlier rejection method were addressed in Wang [23] and Firuzabadi and King [30]. On average, six percent of the total measurements are removed as outliers in this study.

The PPP solutions are defined in an Earth-Centered-Earth-Fixed (ECEF) Cartesian coordinate (XYZ) system with its origin in the Earth's center of mass. In order to study ground deformation at the Earth's surface, the ECEF-XYZ coordinates are converted to a geodetic orthogonal curvilinear coordinate system (longitude, latitude, and ellipsoid height) referencing the GRS80 ellipsoid. The geodetic coordinates with respect to CARIB18 are then projected to a two-dimensional (2D) local horizontal plane. This enabled us to track superficial ground deformation in the north-south (NS) and east-west (EW) directions at each site. The vertical displacement derived from the ellipsoid heights is used to depict land subsidence and uplift in this study. According to the investigation by Wang and Soler [31], the vertical displacement derived from ellipsoid heights retains the same value as those derived from orthometric heights.

It is worth noting, however, that JPL combined numerous redundant regional GPS networks to calculate precise GPS orbit and clock corrections as well as the WLPB estimates that are used by GIPSY during the PPP processing for fixing phase ambiguities. Accordingly, the PPP method essentially relies on observations from a huge number of ground GPS stations, although the end users do not need to

include any data from other ground GPS stations in their PPP processing. There are nine IGS track stations within the Caribbean region (Figure 1), which are used to determine the final satellite orbits and clock corrections by IGS.

3. A Method for Realizing a Stable Reference Frame

The determination of site position at a specific epoch, and in turn, the change of the position over time (site velocity), is the primary task in geological hazard monitoring using GPS. The position and velocity are always determined in a specific reference frame. A stable reference frame indicates that regional "common" movements have been removed or minimized. The regional common movements may include a combination of secular plate motions, glacial isostatic adjustment, surface mass loading, and other minor secular effects [32].

3.1. Seven-Parametric Positional Time Series Transformation

The main physical and mathematical properties of a reference frame are the origin, the scale, the orientation, and the change of these parameters over time. In the geodesy community, a regional reference frame is often developed through a simultaneous transformation from a well-established and broadly used global reference frame, such as IGS reference frames. A group of common points (reference stations) are used to tie these two reference frames. The Helmert coordinate transformation method is often used to produce a distortion-free transformation between two reference frames. The transformation can be realized by a daily 7-parametric transformation method or a 14-parametric transformation method. The 7-parameters include three translations, three rotations, and one scale for each epoch (mostly each day); the 14-parameters include three translations, three rotations, one scale, and their one-time derivatives. For example, a daily 7-parametric method is employed by Blewitt et al. [33] in transforming IGb08 coordinates to the North American Reference Frame of 2012 (NA12) coordinates; a 14-parametric method is employed by NGS in transforming IGS08 coordinates to NAD83 coordinates [34]. The Helmert coordinate transformation method also provides an approach of realizing a regional reference frame by obtaining daily 7-parameters or by obtaining a total of 14-parameters.

The coordinate transformation of a point at a specific epoch from a global (G) reference frame to a regional (R) reference frame can be realized by a combination of rotation, scaling, and translation:

$$P_R = T + (1 + s)RP_G, \tag{1}$$

where P_G represents the positional vector with respect to the global reference frame (e.g., IGS14); P_R represents the transformed positional vector with respect to the regional reference frame (e.g., CARIB18); T is a vector consisting of three translation parameters along the x, y, and z axes; R is a rotation matrix consisting of three rotations around the x, y, and z axes; and s is a scale factor for adjusting the overall distortion that could occur during the transformation. A regional reference frame is often configured to retain the same origin and scale with a global reference frame. Thus, the scale factor s in Equation (1) is often set to zero [34,35]. Accordingly, Equation (1) can be simplified as

$$P_R = T + RP_G, \tag{2}$$

which can be written in an explicit format:

$$\begin{aligned} X(t)_R &= T_x(t) + X(t)_G + R_z(t)\cdot Y(t)_G - R_y(t)\cdot Z(t)_G \\ Y(t)_R &= T_y(t) - R_z(t)\cdot X(t)_G + Y(t)_G + R_x(t)\cdot Z(t)_G \\ Z(t)_R &= T_z(t) + R_y(t)\cdot X(t)_G - R_x(t)\cdot Y(t)_G + Z(t)_G, \end{aligned} \tag{3}$$

where $X(t)_G$, $Y(t)_G$, and $Z(t)_G$ are the ECEF-XYZ coordinates (at epoch t) of a site with respect to the global reference frame; $X(t)_R$, $Y(t)_R$, and $Z(t)_R$ are the ECEF-XYZ coordinates of the site with respect to the regional reference frame; T_x, T_y, *and* T_z are three translational shifts between two reference

frames along the x, y, and z coordinate axes; and R_x, R_y, *and* R_z are three rotations around the x, y, and z coordinate axes. These six parameters (T_x, T_y, T_z, R_x, R_x, R_x) can be calculated using selected common points (reference sites) with known coordinates with respect to both the regional and global reference frames. In theory, three references are enough to obtain those six parameters. However, more reference points are often helpful to solve the inverse problem by using the least-squares method and result in a better fitting and more robust coordinate transformation. The selection of reference stations is critical for realizing a stable regional reference frame. A detailed approach for selecting reference stations will be addressed in the next section. This section will focus on the mathematical aspects of realizing a stable reference frame.

According to numerous investigations [36,37], the time series of these six transformation parameters also retain a linear relationship over time. This can be proven by a strict mathematical induction as long as reference points retain linear displacements with regard to the original global reference frame. Thus, the time series of each of these six transformation parameters can be obtained by linear regression, for example:

$$T_x(t) = T_x(t_0) + T'_x \cdot (t - t_0) \tag{4}$$

The translational and rotational parameters at t_0 are zeros since these two reference frames are aligned at epoch t_0 and are referred to the same ECEF-XYZ coordinate system. There are no translations and rotations for coordinates at this epoch. Thus, the coordinate transformation from a global reference to a regional reference frame described in Equation (3) can be rewritten as

$$\begin{aligned} X(t)_R &= X(t)_G + T'_x \cdot (t - t_0) + R'_z \cdot (t - t_0) \cdot Y(t)_G - R'_y \cdot (t - t_0) \cdot Z(t)_G \\ Y(t)_R &= Y(t)_G + T'_y \cdot (t - t_0) - R'_z \cdot (t - t_0) \cdot X(t)_G + R'_x \cdot (t - t_0) \cdot Z(t)_G \\ Z(t)_R &= Z(t)_G + T'_z \cdot (t - t_0) + R'_y \cdot (t - t_0) \cdot X(t)_G - R'_x \cdot (t - t_0) \cdot Y(t)_G, \end{aligned} \tag{5}$$

where T'_x, T'_y, T'_z, R'_x, R'_y, and R'_z are the one-time derivative of $T_x(t)$, $T_y(t)$, $T_z(t)$, $R_x(t)$, $R_y(t)$, and $R_z(t)$, respectively. $X(t)_G$,$Y(t)_G$, and $Z(t)_G$ can be obtained by the PPP processing. Accordingly, the coordinate transformation at any epoch from a global to a regional reference frame can be accomplished by knowing a total of seven parameters: t_0, T'_x, T'_y, T'_z, R'_x, R'_y, and R'_z. The detailed method for getting these seven parameters will be introduced in the following.

Since $T_x(t)$, $T_y(t)$, $T_z(t)$, $R_x(t)$, $R_y(t)$, and $R_z(t)$ retain a linear regression over time, T'_x, T'_y, T'_z, R'_x, R'_y, and R'_z can be obtained by just knowing the values at any two specific epochs, such as t_0 and t_1. Fox example, T'_x can be calculated by the following equation:

$$T'_x = \frac{T_x(t_1) - T_x(t_0)}{t_1 - t_0} \tag{6}$$

As aforementioned, the translational and rotational parameters at t_0 are zero since there are no translations and rotations of coordinates at t_0. Thus, knowing those six transformation parameters (three translations, three rotations) at one epoch (t_1) is enough to estimate T'_x, T'_y, T'_z, R'_x, R'_y, and R'_z. A strict stable reference frame means that a stable site would retain a zero site velocity over time. Since the stable regional reference frame is tied to a global reference frame at t_0 (e.g., 2015.0), the ECEF-XYZ coordinates of the selected reference sites at epoch t_1 (e.g., 2018.0) with respect to the regional reference frame can be estimated by the following equations:

$$\begin{aligned} X_R(t_1) &\approx X_R(t_0) = X_G(t_0) \\ Y_R(t_1) &\approx Y_R(t_0) = Y_G(t_0) \\ Z_R(t_1) &\approx Z_R(t_0) = Z_G(t_0) \end{aligned} \tag{7}$$

$X_G(t_0)$, $Y_G(t_0)$, $Z_G(t_0)$, and $X_G(t_1)$, $Y_G(t_1)$, $Z_G(t_1)$ can be obtained by the PPP processing. Thus, these six parameters (T_x, T_y, T_z, R_x, R_y, and R_z) at epoch t_1 can be obtained according to Equation (5). Finally, T'_x, T'_y, T'_z, R'_x, R'_y, and R'_z can be estimated according to the method illustrated by Equation (6).

3.2. Selection of Reference Stations

In general, there is no rigorous criterion for selecting reference stations. Some useful guidelines for selecting reference stations have been addressed by a great number of publications [38–40]. The essential criterion is that a reference site should have long-term continuous GPS observations that will allow precise delineations of long-term secular plate motions. However, there is no unified definition for "long-term". According to our experience for realizing stable reference frames within the Houston metropolitan area [41,42] and the North China region [29], a minimum of 3 years continuous observational time span is needed for assessing the linearity of the GPS-derived displacement time series. Linearity is a term that is often used to assess the quality of a potential reference station, which reflects how well the motions can be described by a constant velocity over a period of time.

In practice, the selection of reference stations largely depends on what is available. Different versions of Caribbean reference frames had been realized and applied in previous tectonic studies. For example, DeMets et al. [43] used site velocities from 13 GPS sites to model the movement of the Caribbean plate with respect to ITRF2000; the model was updated with site velocities from 16 GPS sites (12 are campaign stations; 4 are continuous stations) by DeMets et al. [44]. Symithe et al. [45] used more GPS stations to establish a Caribbean reference frame. Those reference frames were designed to map the strain in the Earth's crust at plate boundaries and to "observe" long-term plate or sub-plate motions. They do not provide easy access for non-expert users. Since the advent of GPS, expert users in geodesy often realize their own Caribbean reference frames to define site positions and velocities for tectonic studies; non-experts in geodesy just use individual references to get relative positions. As a consequence, it is difficult to compare and integrate GPS-derived results (e.g., faulting, micro-plate motions, post-seismic deformation) from different researchers obtained during different periods.

The stable portion of the Caribbean plate is covered by water. Sites within the PBZs experience complex stress and retain different site velocities as a result of inter- and intra-plate interactions. As a consequence, defining and implementing a strict plate-fixed reference frame within the Caribbean region could be a great challenge. The boundaries between the stable portion and the PBZs can rarely be defined with high precision. In general, sites closer to the interior portion of the Caribbean plate are less affected by inter-plate interactions compared to sites further away from the interior portion. Accordingly, the initial screening of reference stations is targeted on those stations that are close to the margins of the interior portion of the Caribbean plate. The stability of a GPS site is difficult to be determined at the level of a few millimeters per year prior to having a stable regional reference frame. For this reason, the initial selection of reference stations is mainly based on the geographic distribution and data history rather than "tectonic stability".

Initially, thirty-two stations adjacent to the margins of the interior portion of the Caribbean plate are selected as reference stations (Figure 2a). Stations with an observational period less than three years or have large data gaps have been excluded from the initial selection. The seven parameters (t_0, T'_X, T'_Y, T'_Z, R'_X, R'_Y, and R'_Z) for transforming the positional time series from IGS14 to the interim reference frame are calculated according to the method introduced in the previous section. The XYZ coordinates of each reference station with respect to IGS14 are transformed to the interim reference frame according to Equation (5). The horizontal and vertical site velocity vectors of these 32 reference stations are plotted in Figure 2a. The velocities are referred to the interim reference frame. It is clear that several stations (VRAI, ACP1, CN34, CN36, and SAMA) in the western and southwestern PBZs experienced significantly larger horizontal and/or vertical velocities than the other stations. These stations are affected by the thrust of the Nazca and North Andes plates towards the Caribbean plate (Figure 1). Four stations (CN12, JME2, BAR2, and RDSD) in the northern PBZ also experienced significant horizontal movements with respect to the interim reference frame. Those stations with

large velocities are removed from the group of reference stations and those six parameters (T'_Y, T'_Y, T'_Z, R'_X, R'_Y, and R'_Z) were recalculated. A trial-and-error approach is employed to refine the selection. Stations that have a horizontal velocity higher than 1.5 mm/year or have a vertical velocity higher than 2 mm/year with respect to the new reference frame were removed from the group of reference stations. Finally, eighteen continuous GPS stations were selected as reference stations after several trials and considering the overall geographic distribution of the network of reference stations. Figure 2b depicts the locations of these 18 reference stations and their horizontal and vertical velocity vectors with respect to CARIB18. Four (RDSD, CRO1, LMMF, ABMF) among these 18 reference stations are the IGS tracking stations. The locations of these 18 reference stations, their site velocities with respect to CARB18, and the root-mean-square (RMS) of the detrended displacement time series are listed in Table 1. RMS indicates the precision of the PPP solutions in the Caribbean region. The horizontal precision is approximately 4 mm and the vertical precision is 9 mm. These seven parameters (t_0, T'_X, T'_Y, T'_Z, R'_X, R'_Y, and R'_Z) for transforming the GPS-derived positional time series from IGS14 to CARIB18 are listed in Table 2.

Table 1. Eighteen reference stations and their site velocities with respect to CARIB18.

Reference GPS	Location (Degree)		Site Velocity * (CARIB18, mm/year)			Uncertainty of the Velocity ** (mm/year)			Precision of PPP Solutions *** (RMS, mm)		
	Longitude	Latitude	EW	NS	UD	EW	NS	UD	EW	NS	UD
SAN0	−81.716	12.580	1.1	0.2	0.2	0.2	0.2	0.8	4.8	2.4	7.4
CN35	−81.363	13.376	−0.6	−0.6	−0.4	0.5	0.4	1.2	2.5	2.3	6.9
CN11	−77.784	17.021	−0.5	−0.6	−0.1	0.3	0.3	1.0	2.6	3.3	8.1
CN10	−75.971	17.415	−0.9	−0.6	0.5	0.3	0.3	1.0	2.9	2.6	7.9
CN08	−71.674	17.903	−0.8	−0.6	1.0	0.4	0.4	1.2	3.2	2.6	9.5
CRO1	−64.584	17.757	0.9	−0.6	−1.9	0.2	0.2	0.8	6.5	4.6	11.3
ABMF	−61.528	16.262	0.5	0.1	1.2	0.2	0.3	0.9	3.3	3.0	11.4
LMMF	−60.996	14.595	0.9	−0.1	−1.0	0.3	0.3	1.0	4.9	2.8	10.8
GRE0	−61.640	12.222	0.7	−0.2	−1.2	0.3	0.3	1.0	3.4	2.7	9.5
CN40	−68.958	12.180	0.1	−0.3	1.0	0.3	0.3	0.8	2.2	2.6	9.4
CN19	−70.049	12.612	0.4	1.1	0.9	0.3	0.3	1.1	2.2	2.7	7.6
CN30	−83.772	11.994	−0.7	−0.1	−0.9	0.3	0.3	1.0	3.2	2.9	9.2
CART	−75.534	10.391	−0.4	1.3	−1.4	0.2	0.2	0.6	3.3	7.3	11.1
MIPR	−66.527	17.886	−0.3	0.2	−0.4	0.2	0.2	0.7	2.2	2.0	7.4
SMRT	−63.109	18.042	−0.5	0.6	−0.9	0.2	0.2	0.8	3.9	3.1	10.0
RDON	−62.346	16.934	0.4	0.1	0.6	0.3	0.3	1.0	2.5	2.6	7.7
SVGB	−61.250	13.275	−0.1	−1.1	0.4	0.5	0.4	1.2	5.4	4.1	10.3
CN29	−83.375	14.049	−0.5	0.4	0.4	0.3	0.5	1.3	2.4	2.5	9.1
Root Mean Square:			0.7	0.7	0.9	0.3	0.3	1.0	3.6	3.5	9.2

* The velocity is obtained by a least-squares regression method.
** The uncertainty represents the 95% confidence interval of the velocity estimate.
*** The root-mean-square (RMS) is calculated from the detrended displacement time series.

Table 2. Seven parameters for realizing CARIB18 and PRVI18.

7—Parameters *	Unit	IGS14 to CARIB18	IGS14 to PRVI18
t_0	Year	2015.0	2015.0
T'_x	m/year	−1.4356361E−03	2.5859127E−03
T'_y	m/year	−1.4676530E−03	−2.3777146E−02
T'_z	m/year	−3.2413979E−03	−7.0144708E−02
R'_x	radian/year	7.1428740E−11	1.0791183E−08
R'_y	radian/year	−4.0966177E−09	−1.2130266E−09
R'_z	radian/year	2.5004835E−09	2.0400242E−09

* Those seven parameters are used to transforming IGS14 coordinates (ECEF-XYZ) to CARIB18 and PRVI18 reference frames according to Equation (5).

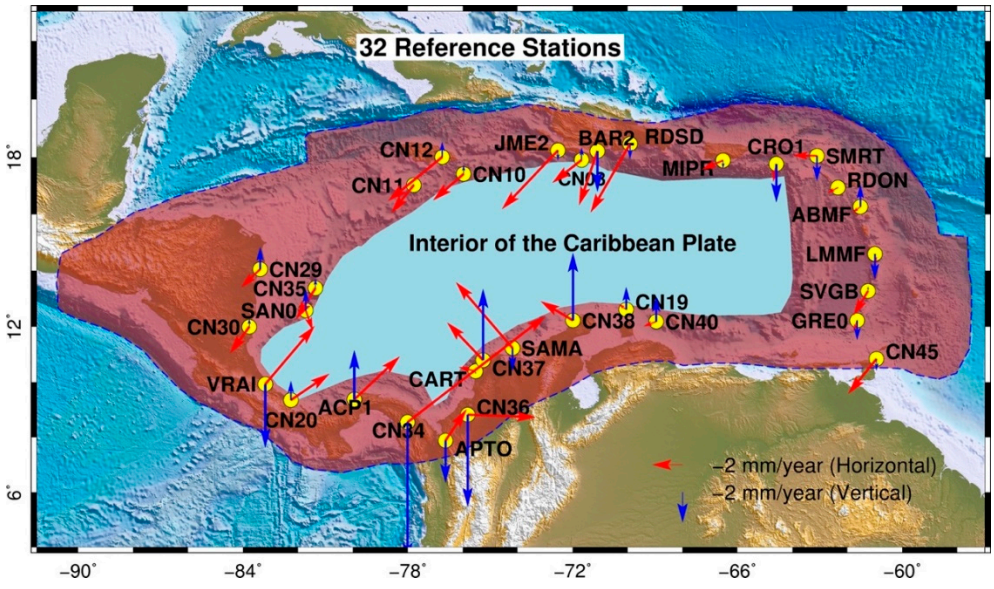

(**a**)

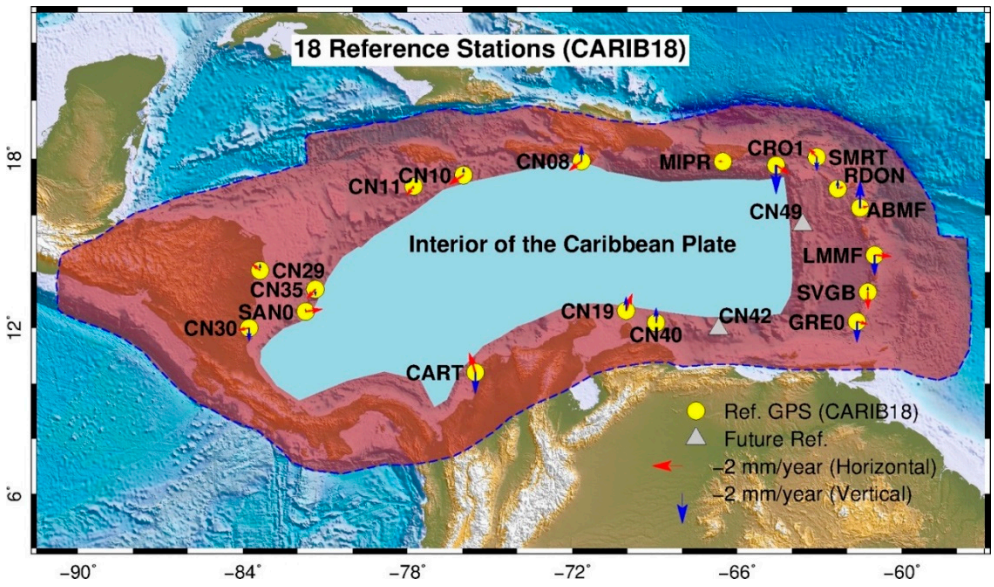

(**b**)

Figure 2. (**a**) Locations of 32 initially selected reference stations for realizing a regional reference frame within the Caribbean region. The horizontal (red) and vertical (blue) velocity vectors are referred to the initial reference frame realized by these 32 reference stations. (**b**) Locations of 18 reference stations for realizing the stable Caribbean reference frame (CARIB18). The horizontal (red) and vertical (blue) velocity vectors are referred to CARIB18.

Figure 3 illustrates the observational history and data continuity of 16 among these 18 reference stations utilized to realize CARIB18. All reference stations have a history of over five years except two COCONET stations: CN29 and CN35. The three-component positional time series of the other two reference stations, CART and CN11, are illustrated in Figures 4 and 5, respectively. CART is a long history (2002–2018) GPS station operated by the Geographic Institute Agustín Codazzi of Colombia (IGAC). CART is kept as a reference station because of its critical geographic location, lying on the continental shelf of South America plate, and filling a large gap of the reference network in the south-west PBZ. CART is not considerably affected by the thrust of the North Andes plate

and the Nazca plate towards the Caribbean plate. All other nearby stations in the southwestern PBZ are significantly affected by the thrust of the two tectonic plates as shown in Figure 2a. Figure 6 illustrates the three-component displacement time series (CARIB18) of another long-term reference station CRO1 (2002–2018). CRO1 is located on St. Croix Island and retains a slightly larger vertical velocity (–1.9 mm/year) compared to other reference stations. A closely spaced permanent GPS station (VIKH) on St. Croix recorded an identical site velocity with CRO1. The slight subsidence recorded by CRO1 may imply minor relative tectonic motions between St. Croix Island and the stable portion of the Caribbean plate.

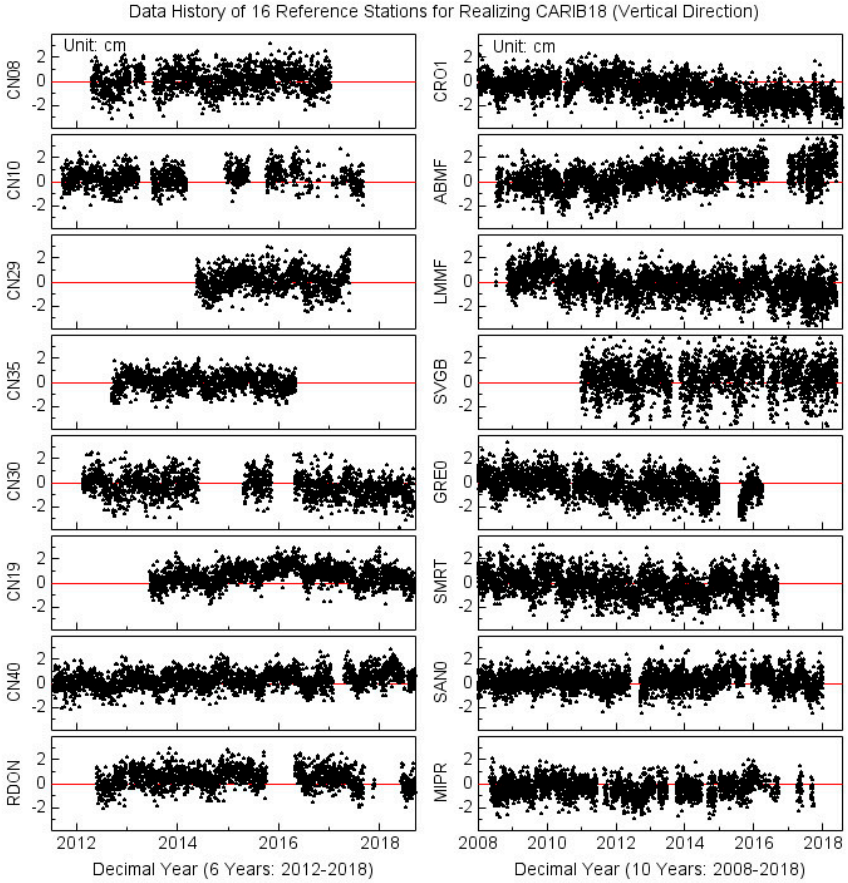

Figure 3. Plots showing the observational history and data continuity of 16 among 18 reference stations for realizing the Stable Caribbean Reference Frame (CARIB18).

Figure 5 depicts the long-term three-component displacement time series at CN11 (2012–2018) and ISCO (2011–2018) with respect to IGS14 and CARIB18. CN11, one of the reference stations for realizing CARIB18, is a COCONET station located on the San Pedro Caye, Jamaica. The 7-year observations indicate that this site moves to the northeast direction with a velocity of approximately 12 mm/year with respect to IGS14. Its three-component velocities (<1 mm/year) with respect to CARIB18 indicate that this site is fixed to the stable portion of the Caribbean plate and is not affected by local faulting activities. ISCO is a COCONET regional station located on the Isla del Coco (Coco Island), the only land mass of the Cocos plate that emerges above sea level. ISCO recorded the largest horizontal velocities with respect to both IGS14 (NS: 73.8 ± 0.5 mm/year; EW: 49.2 ± 0.5 mm/year) and CARIB18 (NS: 69.6 ± 0.5 mm/year; EW: 34.3 ± 0.5 mm/year) within the Caribbean region. The horizontal velocity vector with respect to CARIB18 indicates that the convergence rate of Cocos plate with the Caribbean plate at this site is at 77.6 ± 0.5 mm/year with an azimuth of 26.23 degrees (clockwise direction of North). The observed convergence rate at this site agrees well with the convergence rate estimated by the MORVEL plate motion model [44]: 77.7 ± 2.7 mm/year with an azimuth of 26.9 degrees.

The MORVEL-estimated relative velocity between the Cocos plate and the Caribbean plate is based on an average over the last 780,000 years (the width of the central magnetic anomaly). MORVEL is primarily a geological estimate of plate motions. The consistency between the geological-estimate and the 8-year GPS estimate suggests that the collision between the Cocos and Caribbean plates have been continuing over seven hundred thousand years with a steady velocity. This explains why there are few stable sites within the western PBZ with respect to the interior of the Caribbean plate.

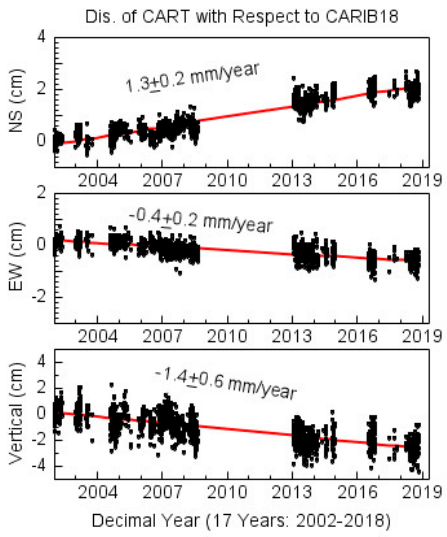

Figure 4. Three-component displacement time series of the long-history GPS station CART with respect to CARIB18. CART is located in Cartagena, Colombia (Figure 2) and is operated by the Instituto Geografico Agustin Codazzi, Colombia.

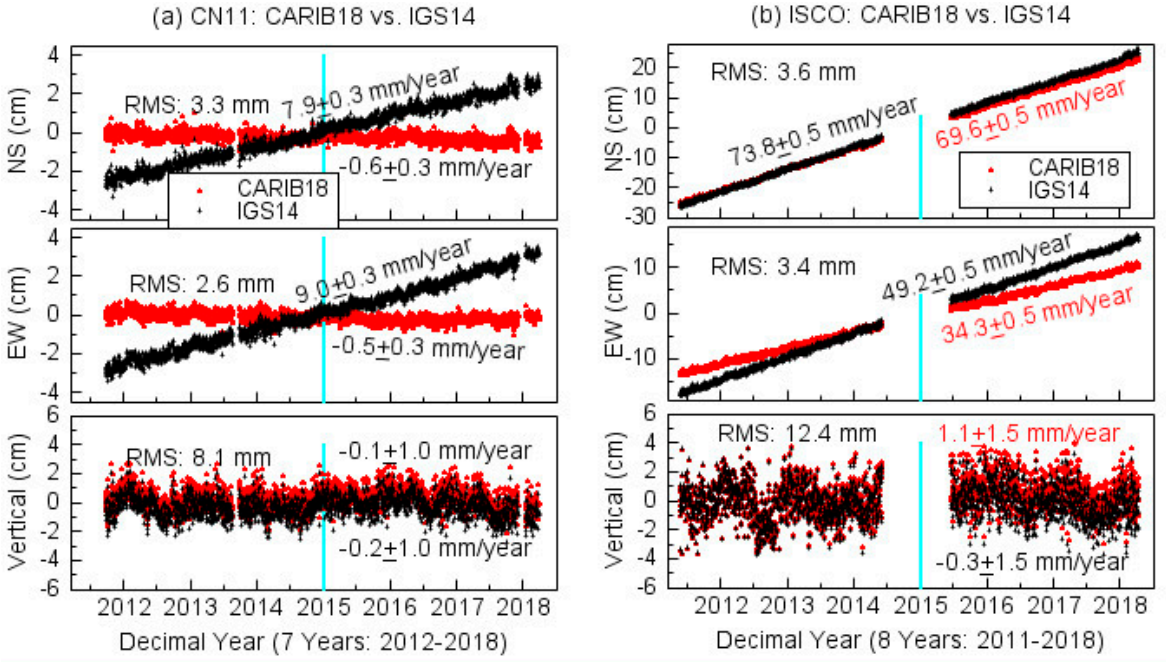

Figure 5. (**a**) A comparison of the displacement time series of CN11 with respect to CARIB18 and IGS14; (**b**) a comparison of the displacement time series of ISCO with respect to CARIB18 and IGS14. The root-mean-square (RMS) of the displacements is calculated from the detrended PPP daily solutions.

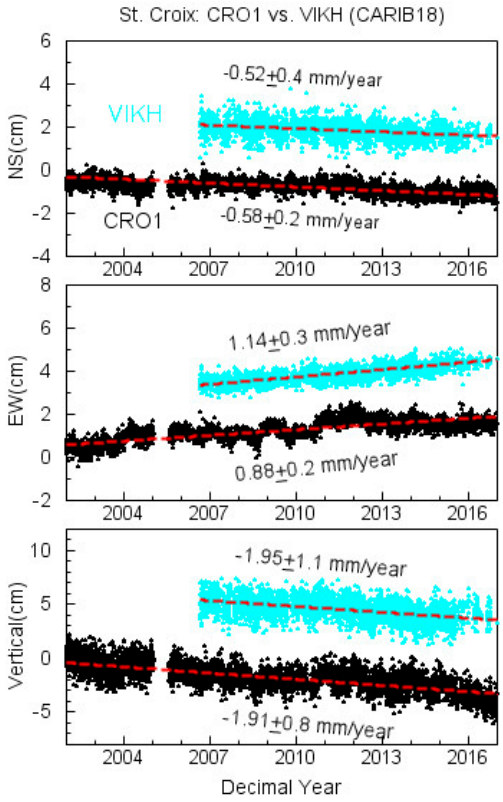

Figure 6. Three-component site velocities with respect to CARIB18 recorded by two permanent GPS stations (CRO1 and VIKH) on St. Croix island. The distance between these two stations is approximately 23 km.

3.3. Effects of Network Geometry

The geometry of the network of reference stations has been recognized as a major element affecting the overall stability of a regional reference frame [35,46,47]. Ideally, the selected reference stations should be evenly distributed over the whole area of interest. Figure 2b indicates that over one-third of these 18 reference stations are located within the eastern PBZ; few reference stations are located within the western and southwestern PBZs. The dense reference stations within the eastern PBZ may predominate the reference network and affect the behavior of the reference frame transformation.

In order to assess the potential effect of the geometry of reference stations on the overall performance of the reference frame, we recalculate these seven parameters by removing two stations (RDON and SVGB) in the eastern PBZ from the network of 18 reference stations and by adding one station (CN20) in the western PBZ to the reference network. CN20 is a COCONET station located on Bocas Island, Panama (Figure 2a). It is close to the interior of the Caribbean plate and is less affected by the thrust of the Cocos plate compared to other stations within the western PBZ. Figure 7 depicts the three-component displacement time series of CN20 with respect to four reference frames realized by 32 reference stations (Figure 2a), 18 reference stations (Figure 2b), 16 reference stations (excluding RDON and SVGB from those 18 stations), and 19 reference stations (adding CN20 to those 18 reference stations). We also checked velocity vectors of other stations with respect to these different reference frames. It is confirmed that adding one station in the western PBZ or removing two or more stations in the eastern PBZ does not considerably degrade the overall stability of the reference frame. The stability of the reference frame will be defined in the next section.

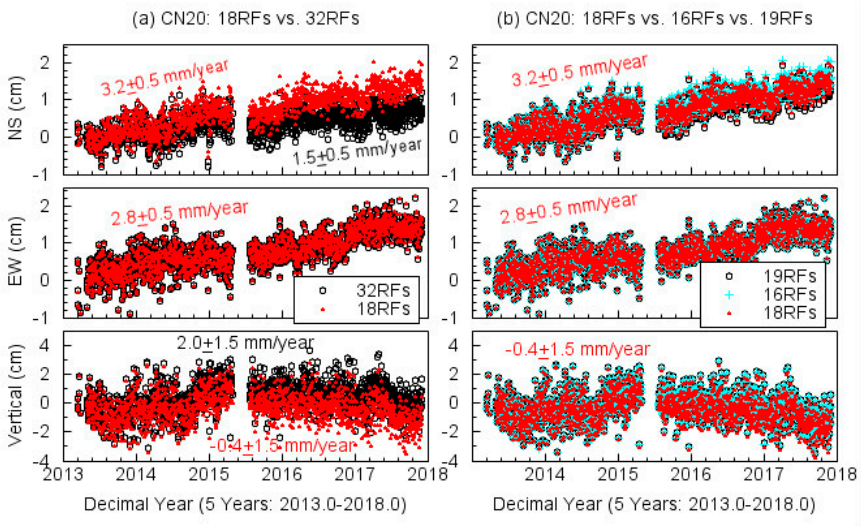

Figure 7. Plots depicting the effect of geometry of reference stations to the stability of the regional reference frame. COCONET station CN20 is located on Bocas Island in Panama (see Figure 2a). (**a**) The three-component displacement time series with respect to the initial reference frame realized by 32 reference stations (Figure 2a) and 18 reference stations (CARIB18, Figure 2b); (**b**) the three-component displacement time series with respect to reference frames realized by 18 reference stations (CARIB18, Figure 2b), 16 reference stations (removing RDON and SVGB from these 18 reference stations), and 19 reference stations (adding CN20 to these 18 reference stations).

3.4. Stability of CARIB18

In practice, a stable site may not retain a near-zero velocity (e.g., <1 mm/year) in 3D space with respect to a stable regional reference frame. For example, stable sites within the Houston, Texas area retain approximately 2 to 3 mm/year horizontal movement towards the northeast direction with respect to NAD83 [48]. NAD83 is regarded as a North American plate fixed reference frame and has been widely applied in both surveying and research communities as a stable reference frame. The 2 to 3 mm/year "background velocity" makes it difficult to use NAD83 as a reference to monitor faulting activities at a few millimeters-per-year level. Since a tectonic plate is not rigid, there is no way to achieve a strictly stable reference frame. To the most stringent users, the stability of a reference frame defines the essence of a successful reference frame. In practice, the stability or precision of a regional reference frame is often evaluated by averaging the velocities of all reference stations with respect to the reference frame [33]. The stability indicates the ability to extrapolate station coordinates accurately into the past and the future beyond the frame range. For CARIB18, the frame range is approximately from 2008 to 2018 as shown in Figure 3. The useful lifetime of a regional reference frame depends on its stability, which is also referred to as predictability. According to the statistics listed in Table 1, the precision of PPP solutions is approximately 4 mm in the horizontal directions and 9 mm in the vertical direction within the Caribbean region; the stability of CARIB18 is at a level of 0.7 mm/year in the horizontal direction and approximately 0.9 mm/year in the vertical direction. That means the reference frame may result in an accumulated positional-error (uncertainty) of 4 mm in the horizontal direction and 5 mm in the vertical direction within a five-year period, which are still below the precision (repeatability) of the PPP daily solutions. That is to say, the regional reference can be confidently used for at least five years beyond the frame window (2008–2018) without causing any considerable positional errors. The stability may be further improved in future updates when a longer time span of observations and more reference stations are used in realizing the regional reference frame.

Ultimately, the stability of a regional reference frame is determined by the rigidity of the block of crust that the reference stations are mounted on. The rigidity of tectonic plates is an important assumption for plate reconstructions and geodynamic modeling [38,49]. The assumption is useful

but not true. In general, a smaller portion of a plate is more appropriate to be considered as a rigid block than a larger portion. Thus, a local-scale reference frame may provide a more stable reference than a regional-scale reference frame and, in turn, is preferred for monitoring local-scale ground deformation over time and space. A dense GPS network has been operated in the Puerto Rico and Virgin Islands (PRVI) region for over ten years [46]. A local-scale reference frame, stable Puerto Rico and Virgin Islands Reference Frame (PRVI12), was established by Wang et al. [34] for landslide monitoring. Seven reference stations with a history of five years were used to realize PRVI12, which achieved stabilities of approximately 1.5 mm/year in both horizontal and vertical directions. PRVI12 was updated to PRVI14 in 2016 by using three more reference stations and a longer period of GPS observations [46]. The stability of PRVI14 was 0.4 mm/year in the horizontal direction and 0.6 mm/year in the vertical direction. We updated PRVI14 to PRVI18 through this study by using three more years of GPS observations and add CN03 to the network of reference stations (Figure 8). CN03 is a COCONET station that was installed on the Virgin Gorda Island in February 2013. The seven-parameters for transforming IGS14 coordinates to PRVI18 are listed in Table 2. The stabilities of PRVI18 are approximately 0.4 mm/year in the horizontal directions and 0.5 mm/year in the vertical direction. The update from PRVI14 to PRVI18 does not considerably improve the stability of the local reference frame, which implies that the stability of PRVI18 is approaching the rigidity of the PRVI block. Adding more reference stations and/or using longer periods of observations may not considerably improve the stability of the local reference frame. The stability of PRVI18 is approximately two times better than the stabilities of CARIB18. This confirms that a reference frame covering a smaller area retains higher stability than a reference frame covering a larger area.

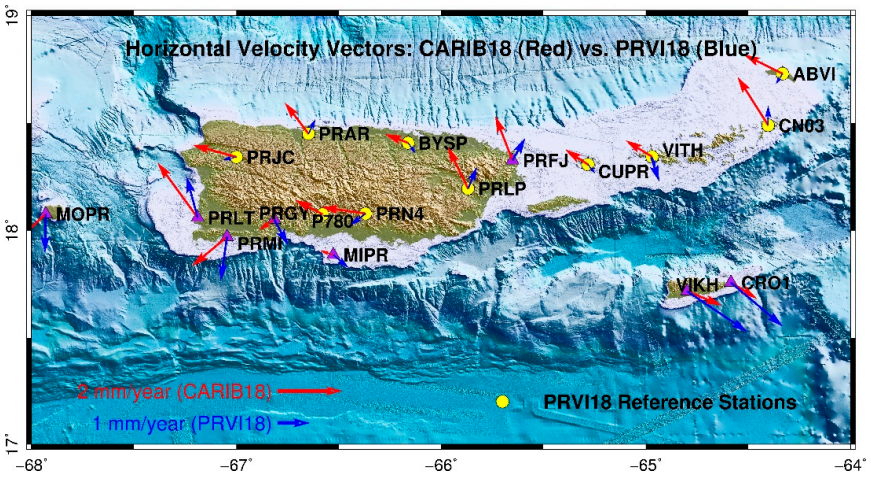

Figure 8. Site velocity vectors of permanent GPS stations on the Puerto Rico and Virgin Islands (PRVI) with respect to the local-scale reference frame PRVI18 (blue) and the regional-scale reference frame CARIB18 (red). The yellow dots represent these 10 reference stations used in realizing PRVI18.

Figure 8 depicts the horizontal velocity vectors of those PRVI GPS stations (>5 years) with respect to CARIB18 (red) and PRVI18 (blue). The magnitudes and directions of the velocity vectors with respect to PRVI18 clearly indicate that those sites (PRMI, PRLT, PRGY) at the southwest corner of the Puerto Rico main island experience substantially larger motions compared to other stations. The horizontal velocities of other GPS stations are at a level of below 0.5 mm/year. However, the horizontal velocities of PRMI and PRLT are at the level of 1.5 to 2 mm/year. PRMI moves southwest against the PRVI block and PRLT moves to the northwest. PRMI is located on Magueyes Island, a small island 2 km south to the southern boundary of Lajas Valley, which is a 30-km-long east–west trending depression zone bounded by hills on its northern and southern edges. This area has the most frequent onshore microseismicity in the PRVI region [50]. Previous researchers have recognized possible Quaternary fault controls for the Lajas Valley on the basis of geomorphology and seismic reflection profiles [51,52].

The velocity anomalies (both magnitude and direction) at PRMI and PRLT confirms ongoing faulting activities within the Lajas Valley. It appears that the Lajas Valley currently experiences a north–south direction extension (1.5 mm/year) and minor right-lateral strike slip. However, the faulting movements are not so obvious with respect to CARIB18 since all stations in the PRVI region retain a horizontal velocity of approximately 1.5 to 2 mm/year. PRVI18 is definitely a better reference frame than CARIB18 for precisely tracking faulting activities and for assessing present seismic risk within the PRVI region.

4. Applications of CARIB18

CARIB18 provides a unified stable reference to study inter-plate motions between the Caribbean plate and its surrounding plates and micro-plate motions within the PBZs. Figure 9 depicts horizontal and vertical velocity vectors derived from GPS observations within the Caribbean region with respect to CARIB18. To ensure reliable tectonic interpretation, we only retain sites that have been continuously recording over three years. The velocities are calculated with the Median Interannual Difference Adjusted for Skewness (MIDAS) method introduced by Blewitt et al. [53]. We visually inspected each displacement time series and corrected obvious errors associated with antenna changes and outliers. We also compared the site velocities calculated by the MIDAS method and the conventional least-squares method. It is found that the velocities obtained by the two methods agree well in general and the MIDAS method does a better job in minimizing the effects of outliers and step discontinuities associated with antenna changes or co-seismic displacements. Locations, observational histories, and three-component velocities with respect to CARIB18 of these 250 stations are listed in Table A1. Site velocities of stations on the Nicoya Peninsula, northwest Costa Rico are derived from GPS observations since 2015. The positional time series during the period from 2012.5 to 2015.0 are significantly affected by the pre-seismic, co-seismic, and post-seismic events associated with the 5 September 2012 Nicoya, Costa Rica earthquake (M_w 7.6) as shown in Figure 10.

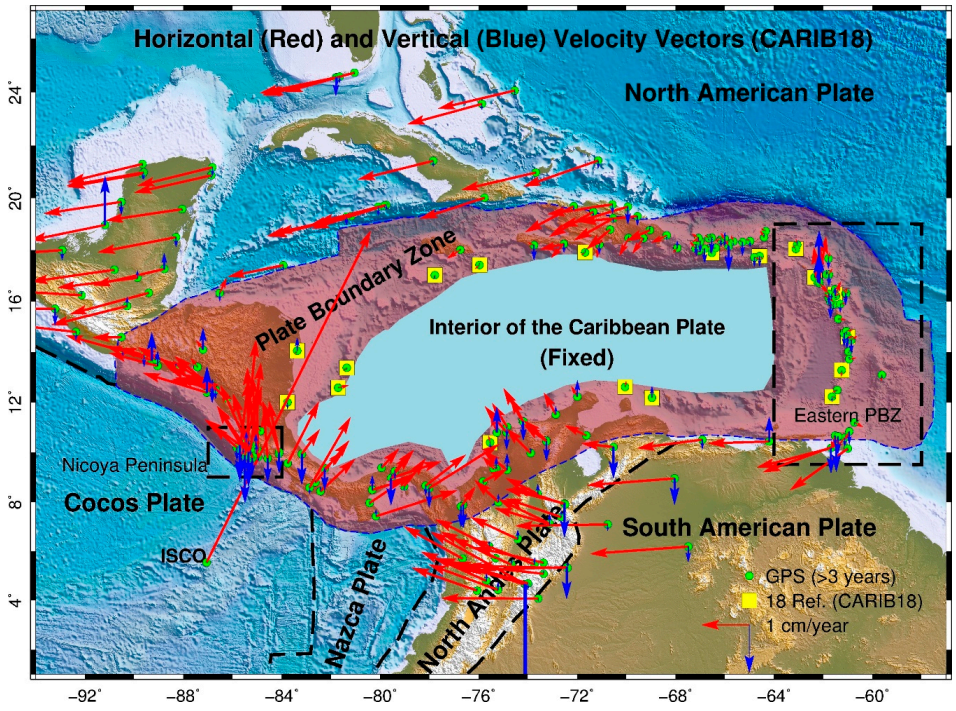

Figure 9. Map showing the horizontal (red) and vertical (blue) velocity vectors at 250 GPS stations with respect to CARIB18. The linearity of the positional time series of GPS stations on the Nicoya Peninsula, northwest of Costa Rica, is affected by the 2012 Nicoya, Costa Rico earthquake (M_w 7.6, 5 September 2012), post-seismic deformation, and slow slip events. Only the observations after 2014.5 are used to calculate the site velocities on the Nicoya Peninsula.

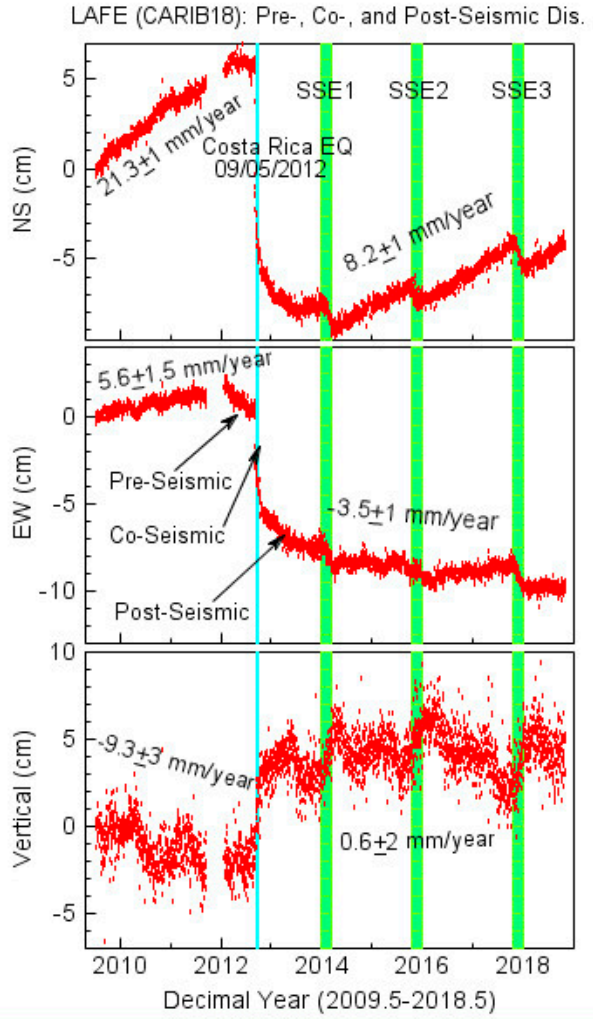

Figure 10. Plots illustrating the application of CARIB18 in delineating pre-seismic, co-seismic, and post-seismic ground deformation associated with the 5 September 2012 Nicoya, Costa Rico earthquake (M_w 7.6), and slow-slip events (SSE). LAFE is located in the small town of Paquera on the Nicoya Peninsula, Costa Rica.

The resulting velocities depicted in Figure 9 show a number of important features. There are strike-slip faults along the northern and southeastern boundaries of the Caribbean plate, allowing westward movements of the North American and South American plates relative to the Caribbean plate. There are little relative motions presently between North and South American plates. The northern PBZ is affected by a left-lateral motion between the Caribbean and North American plates. The southern PBZ is affected by right-lateral motion between South American plate and Caribbean plate, and by northwest thrust movements between the North Andes plate and the Caribbean plate. The western PBZ is occupied by Central America. The Cocos plate and Nazca plate in the Pacific Ocean thrust towards the Caribbean plate. The stations within the western PBZ experience a steady horizontal movement (1–2 cm/year) towards the interior of the Caribbean plate. The eastern PBZ is an island arc which follows the line of the subduction zone where Atlantic plate is being pushed under the Caribbean plate. The site velocities with respect to CARIB18 within the eastern PBZ are less than 1 mm/year except on Monserrat island. Overall, the eastern PBZ shows little movement with respect to the interior of the Caribbean plate. Thus, CARIB18 would be able to serve as a rigorous reference frame for landslide, faulting, subsidence, and volcano and structure health monitoring on these islands, and would be particularly important for land surveying projects on those islands that do not have

long-history GPS stations, such as Dominica, St. Vincent and the Grenadines, and Grenada. The site velocities within the northern, southern, and western PBZs vary from a few millimeters per year to a couple of centimeters per year, which depicts significant microplate motions. Accordingly, CARIB18 may not be a precise reference frame for tracking localized horizontal ground deformations within the northern, southern, and western PBZs. Local-scale reference frames are needed to conduct precise faulting and landslide monitoring on these islands.

Intra-plate motions within the PBZs have been heavily investigated by numerous researchers using GPS observations [54–58]. With the continuous accumulation of COCONET and other GPS observations in and around the Caribbean plate, the research community will soon gain a better understanding of the tectonic motions within the PBZs. Instead of exploring the details of plate tectonic motions, this study will demonstrate the applications of CARIB18 in tracking localized ground deformation for geological hazard monitoring purposes.

4.1. Post-Seismic Monitoring

Post-seismic ground deformation following large earthquakes can occur many years to several decades and affect exceptionally large areas. For example, post-seismic ground deformation following the 1964 Alaska earthquake (27 March 1964, Mw 9.2) is still ongoing even a half-century after the main shock [59,60]. Monitoring post-seismic deformation is critically important to understanding the process of earthquake cycles and improving risk assessment for large earthquakes and tsunami potential. GPS has become an important tool for monitoring post-seismic ground deformation due to after-slip, viscoelastic relaxation, poroelastic rebound, and other slow displacements following large earthquakes. Long-term GPS observations have advanced both the spatial and temporal characteristics of post-seismic deformation.

Earthquakes are the major destructive form of natural hazards in the Caribbean region. The most recent devastating earthquake occurred in the Caribbean region is the 2012 Nicoya, Costa Rica earthquake (M_w 7.6, 5 September 2012). The epicenter of this earthquake was on the Nicoya Peninsula, 11 km east-southeast of Nicoya. This earthquake was felt all over Costa Rica as well as in Nicaragua, El Salvador, and Panama. It was the second strongest earthquake recorded in Costa Rica's history, following the 1991 Limon earthquake (M_w 7.7, 22 April 1991). Figure 10 illustrates the application of CARIB18 in depicting pre-seismic, co-seismic, and post-seismic ground deformation associated with the mainshock. LAFE is located on the Nicoya Peninsula, northwestern Costa Rica. Ongoing post-seismic deformation and three slow-slip-events (SSE) can be clearly identified from the positional time series with respect to CARIB14. Unfortunately, the SSE events can be barely identified from the positional time series with respect to IGS14. The site velocities before and after this earthquake are considerably different, particularly in the north-south (NS) direction (21 mm/year vs. 8 mm/year), which suggests that the post-seismic deformation is still ongoing at this site. Post-seismic, episodic tremor, and SSE following the 2012 Nicoya earthquake had been investigated by different research groups using GPS data observed during different periods [61–64]. Those results were referred to different reference stations or reference frames. As a consequence, it is difficult to align and compare those results. Figure 11 illustrates the application of CARIB18 in depicting spatial variations of horizontal and vertical ground deformation associated with the pre-seismic, co-seismic, post-seismic, and SSE. CARIB18 provides a unified platform for non-expert GPS users to conduct advanced post-seismic, co-seismic, and SSE modelling over time and space.

4.2. Volcano Monitoring

Volcanoes are distributed all over the Caribbean region. Most of the active volcanoes are located on the Lesser Antilles islands within the eastern PBZ and on the Central American Arc (CAVA) within the western PBZ. The Lesser Antilles has been described as a double island arc that is built largely by volcanism above a subduction zone [65]. CAVA is a chain of volcanoes which extends parallel to the Pacific coastline from Guatemala, El Salvador, Honduras, Nicaragua, Costa Rica, and down

to northern Panama. Presently, the most active volcanos within the Caribbean region are the Fuego Volcano in Guatemala within the western PBZ and the Soufriere Hills Volcano (SHV) on Montserrat Island within the eastern PBZ. Fuego has erupted more than 60 times since 1524, making it Central America's historically most active volcano [66]. The most recent disastrous eruption occurred on 3 June 2018, which was the deadliest eruption in Guatemala since 1929. Unfortunately, there are few long-term permanent GPS stations near the Fuego Volcano.

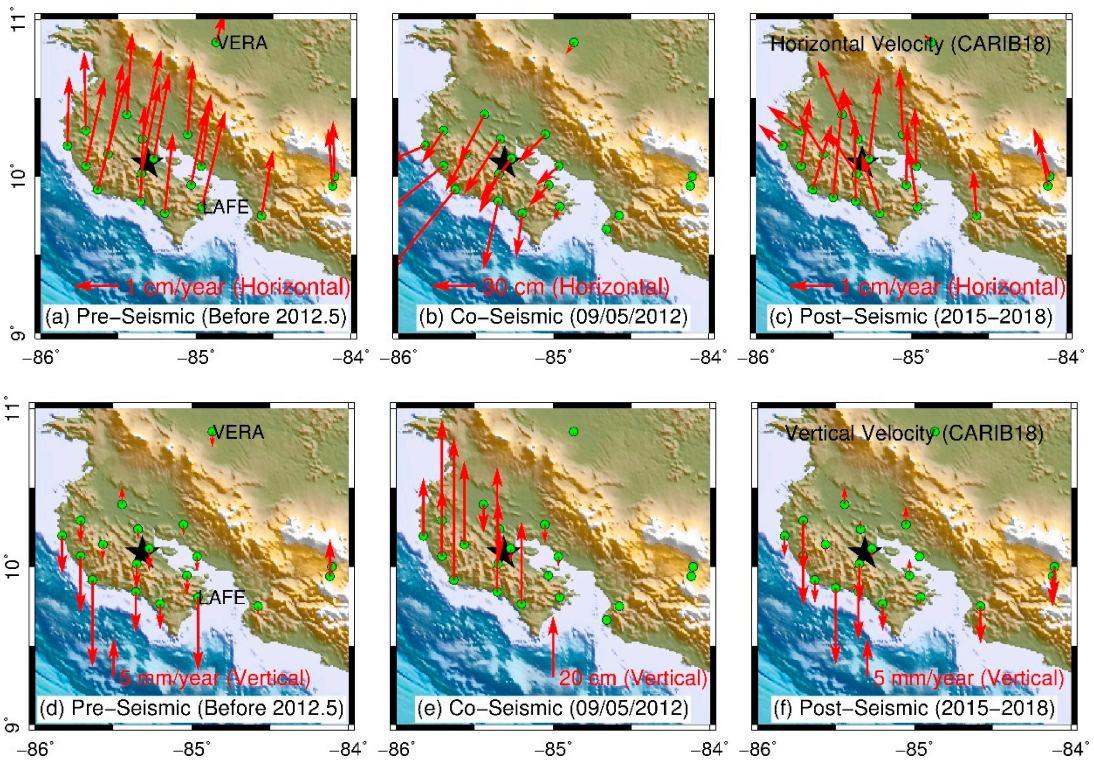

Figure 11. Maps illustrating the application of CARIB18 in depicting spatial patterns of pre-seismic, co-seismic, and post-seismic ground surface deformation caused by the Nicoya, Costa Rica earthquake (5 September 2012; M_w 7.6). (**a**) and (**d**): Horizontal and vertical velocity vectors at GPS stations on the Nicoya Peninsula before the 2012 earthquake; (**b**) and (**e**): Co-seismic displacements occurred during the day that earthquake happened; (**c**) and (**f**): Post-seismic velocity vectors since 2015. The co-seismic displacement is calculated by differencing the one-week average positions after the earthquake day (5 September 2012) and one-week average position before the earthquake day.

This study demonstrates the application of CARIB18 in monitoring SHV within the eastern PBZ (Figure 12). SHV has been one of the most intensively studied volcanoes in the worldwide [67–69]. In the last century, SHV has experienced at least eight aborted eruption events: 1897–98, 1933–37, 1966–67, November 1995–March 1998; November 1999–July 2003; August 2005–April 2007; July 2008–January 2009; and most recently October 2009–February 2010 [70]. Recent eruption events since 2005 can be clearly identified from the long-term continuous GPS observations as illustrated in Figure 13. Ground surface deflates when lava is extruding and then inflates in times of non-extrusion. Changes to the ground surface of a volcano can provide clues about what is happening deep below the surface and provide insightful information of a forthcoming eruption [71–74]. Current ground inflation at a rate of 1 cm/year has continued over nine years since the last eruption in February 2010.

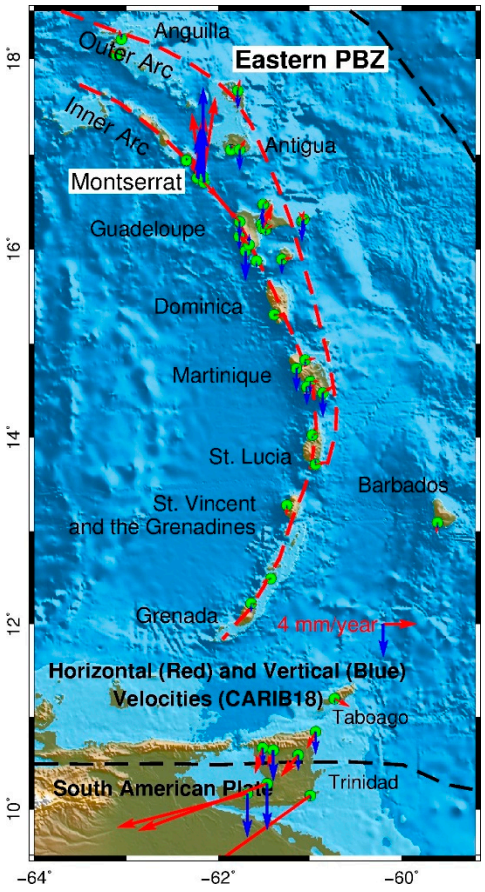

Figure 12. GPS-derived site velocity vectors (red: horizontal; blue: vertical) at permanent GPS stations within the eastern PBZ (Lesser Antilles islands) with respect to CARIB18.

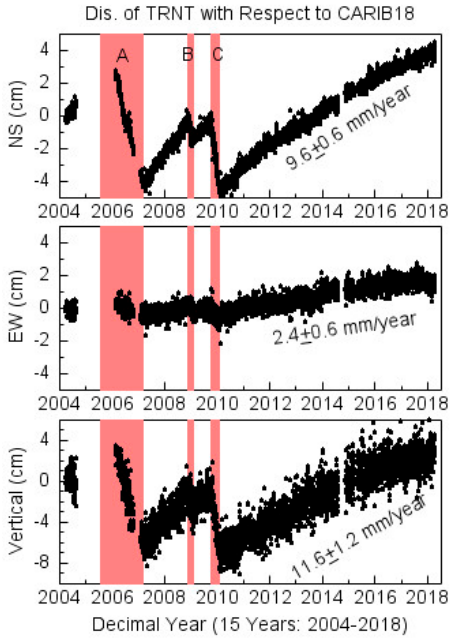

Figure 13. GPS recorded ground deformation associated with the volcanic activities of the Soufriere Hills Volcano on Montserrat since 2004. Shaded A, B, and C periods represent three eruption events. The marked velocity is the linear regression of the displacement time series from 2010 to 2018. TRNT is located about 6 km NNE from the mouth of the volcano (see Figure 14).

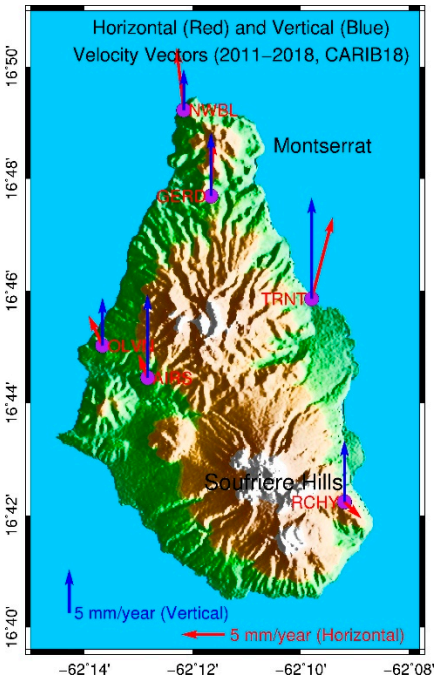

Figure 14. Velocity vectors (red: horizontal; blue: vertical) with respect to CARIB18 at six permanent GPS stations on Montserrat Island. The velocities are derived from GPS observations (2011–2018) after the last eruption of the Soufriere Hills Volcano.

The GPS monitoring at SHV was started by the third author of this article (Dr. Mattioli)) in collaboration with the Montserrat Volcano Observatory (MVO) [75]. Currently, MVO operates a GPS, seismic, and SO_2 integrated monitoring network on Montserrat Island. Figure 14 depicts the ongoing ground deformation velocity vectors (2011–2018) on Montserrat derived from six long-term GPS stations since the last eruption and dome collapse in February 2010. The velocity vectors are referred to CARIB18. Five stations on the north side of the volcano show significant horizontal movements toward the north direction. RCHY lies on the southeast side of the volcano and is close to the volcano mouth. RCHY remains almost stable horizontally (<2 mm/year) with respect to the interior of the Caribbean plate (CARIB18), which suggests that significant horizontal displacements recorded by other GPS stations on the island are induced by shallow magma accumulation under the ground surface rather than tectonic drift. The entire island is still inflating at a rate of approximately 1 cm/year, which suggests that Montserrat's volcano system remains active. There is an increasing interest in projecting when the next major volcanic eruption will occur. Continuous GPS monitoring is vital to understanding whether and when the volcano may become active. CARIB18 provides a coherent reference frame for excluding long-term tectonic drifts from localized ground deformation and enables "absolute" volcano-induced ground deformation monitoring. The absolute ground deformation information will provide a precise estimate of the volume of intrusion magma over time and space.

5. Discussion

This study introduced an approach of using stand-alone GPS and a stable reference frame to conduct long-term geological hazard and structural health monitoring. By transforming PPP solutions to a regional reference fame, users do not need to install any ground reference stations in the field and do not need to include any reference data in their data processing. The stand-alone GPS surveying method will substantially reduce field costs and logistics for conducting long-term ground and structural deformation monitoring and therefore will revolutionize the way for conducting geological hazard and structural health monitoring. Hydrologists may use CARIB18 for studying ground deformations resulting from fluid withdrawal, aquifer deformation, and seasonal hydrologic and atmospheric

pressure loading; geomorphologists may use CARIB18 for studying coastal erosion and wetland loss problems along the Caribbean coasts; oceanographic and sea-level researchers may use CARIB18 for monitoring and calibrating long-term sea level changes along the Caribbean costs; civil engineers may use CARIB18 for monitoring long-term stabilities of dams, sea walls, levees, high-rise buildings, and long-span bridges. It is anticipated that the regional reference frame will promote the applications of GPS techniques in the practice of geological hazard mitigation within the Caribbean region. CARIB18 will also facilitate the applications of GPS technology in construction, land surveying, photogrammetric, coastal hydrography, flooding risk mapping, and natural resource management.

A sophisticated regional geodetic infrastructure would comprise at least two components: a network of numerous permanent GPS stations and a regional reference frame. This study realized a stable regional reference frame that will serve as the essential geodetic infrastructure for long-term geohazards monitoring within the Caribbean region. A longer period of data accumulation from more reference stations would provide more reliable site velocity estimations and, in turn, improve the stability of the reference frame. CARIB18 will be updated periodically with a longer period of data accumulation and additional reference stations to ensure its continuity and stability. There are several other COCONET stations adjacent to the interior of the Caribbean plate that have not been utilized as reference stations in this study because of their short observational histories, such as CN49 and CN42 (Figure 2b). CN49 is located on Aves Ridge, approximately 250 km west of the Lesser Antilles Volcanic Arc. It is much closer to the rigid portion of the Caribbean plate than other stations within the eastern PBZ. Previously, there was a campaign GPS station (AVES) on this island. AVES was used as a reference station by previous investigations [43]. CN42 is located on Gran Roque Island in the southeastern Caribbean Sea, over 200 km off the northeastern coast of Venezuela. CN49 was installed in April 2016 and no data has been archived since the Hurricanes Irma and Maria in 2017. CN42 was installed in October 2015 and no data has been archived since 2017. Those two stations will be considered as reference stations when updating the regional reference frame in the future.

This study confirms that a reference frame covering a smaller area overall retains higher stability than a reference frame covering a larger area. CARIB18 is able to serve as a rigorous stable reference frame for ground and structural deformation monitoring over time and space on the islands of the Lesser Antilles (eastern PBZ). However, it may not be an ideal reference frame for precisely (e.g., <2 mm/year) tracking horizontal ground and structural deformation on the other Caribbean islands. For faulting, subsidence and earthquake monitoring, and risk assessment with the Puerto Rico and Virgin Islands region, we recommend using PRVI18 rather than CARIB18. Rigorous local-scale reference frames require the geodesy community to install and maintain more continuously operating GNSS stations.

6. Conclusions

CARIB18 provides a platform to integrate observations from different remote sensing techniques (e.g., GPS, InSAR, LiDAR, Photogrammetry) to a unified geodetic reference and enables multidisciplinary and cross-disciplinary research. The primary products from this study are the 7-parameters (Table 2) for converting the positional time series from IGS14 to CARIB18 and the three-component velocities of 250 Caribbean GPS stations with respect to CARIB18 (Table A1). Researchers in plate tectonics may use these velocity vectors to study current inter- and intra-plate motions within the Caribbean region. The frame stability of CARIB18 is approximately 0.7 mm/year in the horizontal direction and 0.9 mm/year in the vertical direction. CARIB18 can be confidently used for at least five years beyond the frame window from 2008 to 2018. Current GPS geodesy infrastructure within the Caribbean region makes it possible to precisely track minor ground deformation at the level of 1 mm/year and above using stand-alone GPS. CARIB18 will be synchronized with the update of the IGS reference frame.

Author Contributions: G.W. and H.L. prepared the original draft. All authors edited, reviewed, and improved the manuscript.

Funding: This research was funded by the National Science Foundation (NSF) of the U.S. through the COCONET Award (EAR-1042906), the UNAVCO Operational Award (EAR-0350028), and the Geodesy Advancing Geosciences and EarthScope (GAGE) Award (EAR-1261833).

Acknowledgments: The first author appreciates the Geodesy Advancing Geosciences and EarthScope (GAGE) Facility at UNAVCO and the Nevada Geodetic Laboratory (NGL) at the University of Nevada for sharing their GPS products with the public. The authors acknowledge the NASA Jet Propulsion Laboratory, Caltech, for providing the GIPSY-OASIS software package (V6.4) (https://gipsy-oasis.jpl.nasa.gov) used to generate the PPP solutions for this study. The authors also acknowledge the contributions of COCONET partners (https://coconet.unavco.org).

Conflicts of Interest: The authors declare no conflict of interest.

Appendix A

Table A1. Observational histories and site velocities (CARIB18) of 250 permanent GPS stations within the Caribbean region.

	Long.	Lat.	Start*	End	Observations		Site Velocity (CARIB18) (mm/year) **			Velocity Uncertainty (mm/year) **		
GPS	(Degree)		(Decimal Year)		(Years)	(Days)	EW	NS	UD	EW	NS	UD
AACR	−84.118	9.939	2011.009	2018.834	7.825	2286	−7.5	7.7	−0.3	0.6	0.7	1.5
ABCC	−74.127	4.661	2010.004	2018.839	8.835	1683	−19.0	5.2	−30.1	0.5	0.5	2.0
ABE1	−61.509	16.472	2013.084	2018.839	5.755	1821	0.3	0.7	−1.3	0.4	0.5	1.5
ABMF	−61.528	16.262	2008.539	2018.839	10.300	2040	0.3	0.1	1.3	0.3	0.4	1.2
ABPW	−73.995	4.690	2010.004	2018.839	8.835	1720	−15.7	4.3	−1.5	0.4	0.3	1.1
ABVI	−64.332	18.730	2011.097	2017.243	6.147	2112	−0.9	0.5	0.0	0.4	0.4	1.2
ACHO	−80.173	7.415	2011.387	2016.753	5.366	1708	12.6	5.5	1.1	0.7	0.4	1.4
ACP1	−79.950	9.371	2008.816	2018.839	10.023	2861	3.5	3.9	0.8	0.3	0.3	1.0
ACP6	−79.408	9.238	2008.791	2018.839	10.048	2773	3.8	4.4	−1.8	0.3	0.5	1.3
ADE0	−61.086	16.297	2003.124	2014.995	11.871	2751	0.2	1.2	−2.4	0.4	0.4	1.1
AGCA	−73.595	8.315	2012.394	2018.563	6.168	1017	−7.0	3.2	2.2	0.6	0.6	2.3
AIES	−89.050	13.447	2007.351	2017.799	10.448	3213	−10.2	2.7	3.1	0.3	0.6	0.9
AIRS	−62.214	16.741	2004.233	2018.398	14.166	4155	−0.5	2.4	5.5	0.7	0.5	1.7
ALBI	−61.515	10.663	2007.034	2011.327	4.293	356	−0.9	−3.0	−2.2	0.7	0.8	2.5
ALPA	−72.918	11.528	2015.003	2018.648	3.644	633	−5.3	2.6	−5.1	1.3	0.5	1.8
APTO	−76.632	7.878	2007.836	2018.741	10.905	2081	1.8	3.1	−4.9	0.3	0.4	1.0
ARCA	−70.759	7.084	2008.594	2018.839	10.245	1974	−19.4	−0.5	−1.2	0.3	0.3	1.1
AZUE	−80.433	7.956	2008.580	2012.939	4.359	818	9.0	6.0	−0.4	0.5	0.4	1.5
BAR2	−71.098	18.209	2005.752	2018.839	13.087	3413	−0.6	−2.9	−2.0	0.3	0.3	1.0
BDOS	−59.609	13.088	2004.446	2013.941	9.495	2423	−0.2	−1.3	−0.7	0.6	0.4	1.1
BER1	−74.410	6.493	2007.373	2016.783	9.410	2462	−9.9	4.6	1.9	0.5	0.5	1.8
BGGY	−61.861	17.045	2007.937	2018.839	10.902	3846	0.2	0.5	0.5	0.3	0.3	0.9
BIJA	−84.577	9.750	2009.640	2018.839	9.199	2442	−2.1	8.2	0.8	0.6	1.0	1.3
BNGA	−73.124	7.105	2010.283	2018.839	8.556	1811	−11.6	3.2	2.0	0.5	0.4	1.8
BOGA	−74.080	4.639	2002.001	2018.839	16.838	4997	−20.2	11.1	−43.5	0.2	0.3	1.0
BOGT	−74.081	4.640	2002.390	2018.839	16.449	5659	−15.8	4.8	−35.9	0.2	0.2	1.1
BON2	−85.203	9.765	2004.791	2018.839	14.048	4219	−3.7	12.1	−6.8	1.1	0.7	1.2
BOS1	−73.886	9.967	2012.939	2018.839	5.900	724	−5.7	5.1	0.6	0.4	0.4	1.4
BOU1	−61.770	16.132	2013.383	2018.839	5.457	1159	0.6	−1.0	−2.9	1.5	0.7	4.2
BQLA	−74.850	11.020	2007.765	2018.059	10.294	1576	−3.1	4.9	−2.1	0.4	0.2	0.9
BUC1	−73.119	7.119	2006.004	2009.353	3.348	1072	−10.8	5.1	−0.4	0.5	0.6	1.9
BYSP	−66.161	18.408	2008.348	2018.839	10.492	3538	−0.7	0.2	−1.2	0.3	0.3	1.0
CABA	−85.344	10.238	2009.511	2018.839	9.328	3147	−3.0	11.8	4.8	0.9	0.8	1.5
CALD	−60.731	11.196	2007.028	2011.327	4.298	367	1.8	−0.9	−0.5	0.6	0.7	2.3
CANO	−67.482	6.185	2010.856	2015.151	4.296	345	−20.6	−1.5	−3.2	0.4	0.5	2.5
CAPI	−72.428	5.351	2015.003	2018.248	3.244	565	−21.4	−0.7	−6.6	1.1	0.5	1.9
CART	−75.534	10.391	2002.001	2018.839	16.838	1486	−0.4	1.3	−1.4	0.2	0.2	0.6
CAS5	−75.200	7.989	2008.945	2018.839	9.895	1307	−5.0	4.5	1.7	0.2	0.2	1.0
CBMD	−79.758	19.738	2012.994	2018.839	5.845	1880	−14.9	−4.0	−1.2	0.4	0.4	1.2
CBSB	−79.833	19.712	2005.886	2014.256	8.370	2270	−15.2	−4.8	−0.6	0.3	0.4	1.1
CDM1	−83.764	9.554	2010.308	2015.266	4.958	897	6.6	12.9	0.3	0.5	0.3	0.9
CDTO	−82.873	8.573	2008.583	2015.266	6.683	1641	8.6	14.8	−1.3	0.5	0.5	1.3
CHET	−88.299	18.495	2003.165	2018.834	15.669	4307	−16.5	−3.2	−2.1	0.2	0.2	0.8
CHIN	−81.807	24.550	2008.912	2018.815	9.903	1574	−16.0	−3.5	−3.6	0.3	0.4	1.1
CHIS	−90.291	15.812	2011.140	2015.921	4.780	994	−15.4	−3.1	−0.4	0.7	0.8	2.2

Table A1. *Cont.*

	Long.	Lat.	Start*	End	Observations		Site Velocity (CARIB18) (mm/year) **			Velocity Uncertainty (mm/year) **		
GPS	(Degree)		(Decimal Year)		(Years)	(Days)	EW	NS	UD	EW	NS	UD
CN00	−61.786	17.669	2012.641	2018.839	6.199	1943	−0.3	1.0	−2.5	0.5	0.4	1.2
CN01	−61.765	17.048	2015.077	2018.804	3.726	1202	0.0	0.7	−3.7	0.6	0.6	1.5
CN02	−63.054	18.204	2013.298	2017.678	4.381	1554	−0.2	1.2	0.7	0.5	0.5	1.7
CN03	−64.403	18.490	2013.150	2017.602	4.452	1607	−0.8	1.4	0.7	0.6	0.4	1.6
CN04	−60.974	14.024	2014.196	2018.839	4.643	1433	0.2	−0.1	−1.1	0.6	0.5	2.0
CN05	−68.359	18.564	2014.108	2018.839	4.731	1697	−3.5	−1.7	−0.9	0.4	0.4	1.5
CN06	−70.656	18.790	2012.624	2018.694	6.070	2094	−5.0	−4.3	0.1	0.4	0.5	1.4
CN07	−70.566	19.758	2012.320	2017.769	5.448	1954	−13.6	−2.1	−1.9	0.4	0.4	1.5
CN08	−71.674	17.903	2012.304	2017.024	4.720	1617	−0.8	−0.5	0.6	0.5	0.5	1.8
CN09	−72.140	19.688	2013.489	2018.568	5.079	1708	−10.3	−5.5	−1.1	0.4	0.4	1.5
CN10	−75.971	17.415	2011.718	2017.676	5.958	1301	−0.9	−0.8	0.5	0.4	0.4	1.5
CN11	−77.784	17.021	2011.724	2018.839	7.116	2476	−0.3	−0.7	−0.9	0.3	0.3	1.1
CN12	−76.749	18.004	2012.162	2018.839	6.678	2389	−2.9	−2.0	0.1	0.5	0.5	1.8
CN13	−74.534	24.065	2014.078	2018.839	4.761	1670	−16.4	−4.1	−0.8	0.4	0.4	1.4
CN14	−73.678	20.975	2014.086	2017.676	3.589	1291	−15.6	−3.6	0.1	0.5	0.6	1.8
CN16	−77.850	21.422	2014.385	2018.839	4.455	1560	−16.1	−4.2	−1.2	0.5	0.5	1.5
CN18	−83.944	17.408	2014.741	2018.596	3.855	1308	−11.6	−2.4	−1.1	0.5	0.6	1.9
CN19	−70.049	12.612	2013.457	2018.691	5.235	1893	0.1	1.1	0.1	0.4	0.4	1.3
CN20	−82.256	9.352	2013.202	2018.839	5.637	1904	2.8	2.7	−2.3	0.5	0.5	1.7
CN21	−87.427	13.403	2014.335	2018.314	3.978	1338	−1.4	1.8	−0.2	0.6	0.5	1.9
CN22	−87.045	12.384	2012.110	2014.001	1.892	641	−13.4	4.1	5.4	1.2	1.3	2.8
CN23	−88.779	17.261	2012.570	2018.467	5.897	2085	−14.9	−3.5	3.4	0.6	0.4	1.8
CN24	−88.054	19.576	2013.832	2018.672	4.841	1706	−16.3	−2.3	−0.7	0.5	0.5	1.4
CN25	−92.135	16.232	2014.122	2018.839	4.717	1669	−15.0	0.7	1.2	0.5	0.4	1.6
CN27	−69.940	19.667	2012.632	2018.839	6.207	1964	−14.5	−4.4	−2.7	0.4	0.5	1.7
CN28	−79.034	8.625	2013.202	2018.839	5.637	1896	4.3	5.6	−1.0	0.4	0.4	1.3
CN29	−83.375	14.049	2012.622	2017.407	4.786	1100	−0.4	−0.6	0.7	0.4	0.7	1.9
CN30	−83.772	11.994	2012.121	2018.672	6.552	1841	−0.8	−0.3	−1.5	0.4	0.4	1.3
CN33	−80.327	8.487	2011.866	2017.681	5.815	1410	7.0	2.1	3.0	0.8	0.7	2.0
CN34	−78.015	8.549	2013.183	2017.796	4.613	1639	9.7	9.2	−10.5	2.6	2.2	7.1
CN35	−81.363	13.376	2012.693	2016.337	3.644	1310	−0.6	−0.5	−0.4	0.6	0.5	1.5
CN36	−75.821	8.820	2012.635	2017.875	5.240	1528	5.1	2.6	−0.5	0.6	0.9	2.5
CN37	−75.263	10.793	2012.649	2017.884	5.235	1542	−1.3	3.6	5.3	0.9	0.9	2.5
CN38	−71.988	12.222	2012.665	2016.627	3.962	1420	−1.3	2.2	3.4	0.5	0.4	1.5
CN39	−70.524	10.206	2015.058	2018.834	3.776	1355	−7.3	0.5	−5.4	0.7	0.5	1.7
CN40	−68.958	12.180	2011.554	2018.839	7.286	2517	−0.1	0.4	2.2	0.3	0.3	1.0
CN41	−68.042	8.943	2015.053	2018.839	3.787	1370	−18.7	−1.6	−4.6	0.5	0.5	1.7
CN45	−60.938	10.837	2013.457	2018.114	4.657	1624	−1.0	−2.0	−2.7	0.5	0.7	1.7
CN46	−61.427	12.487	2014.377	2017.832	3.455	795	−1.0	−0.5	0.1	0.5	0.4	2.4
CN47	−60.941	13.711	2014.166	2017.758	3.592	553	1.4	0.3	0.6	0.6	0.7	2.6
CN49	−63.618	15.667	2016.285	2017.659	1.374	408	0.2	−0.3	−12.3	1.7	1.6	6.3
CN53	−72.254	21.783	2015.789	2018.839	3.050	1054	−20.1	−3.6	−3.2	2.8	0.7	1.7
CNC0	−86.821	21.175	2007.425	2018.836	11.411	2883	−15.9	−3.9	−1.9	0.2	0.2	0.7
CNG2	−86.699	12.501	2011.392	2018.026	6.634	1739	−9.0	2.2	−1.9	0.8	0.9	1.5
CNR1	−89.289	13.670	2008.183	2017.317	9.134	3001	−9.3	−3.4	5.9	0.3	0.8	1.2
CORO	−75.288	9.328	2011.992	2016.068	4.077	1231	−2.3	2.2	2.5	0.5	0.5	1.6
CRCS	−66.914	10.503	2009.799	2014.565	4.767	1090	−13.6	−1.8	−2.0	0.6	0.5	2.2
CRO1	−64.584	17.757	2002.001	2018.839	16.838	5743	0.8	−0.5	−2.0	0.3	0.2	0.8
CRSE	−69.044	18.768	2013.517	2018.839	5.322	1641	−5.3	−2.9	0.0	0.5	0.5	1.7
CUC1	−72.513	7.932	2015.003	2018.160	3.157	896	−12.4	3.1	−7.1	0.7	0.8	2.7
CUCU	−72.488	7.898	2004.121	2018.839	14.719	3573	−11.0	3.6	0.3	0.3	0.3	1.2
CUM3	−64.195	10.429	2009.963	2014.565	4.602	797	−12.8	−0.4	15.2	0.5	0.6	2.4
CUPR	−65.283	18.307	2008.835	2017.714	8.879	2685	−0.7	0.4	−2.8	0.3	0.3	1.2
DAR2	−78.154	8.658	2015.422	2018.596	3.173	797	8.5	6.6	14.2	0.8	0.7	7.7
DAV2	−82.434	8.425	2008.600	2018.579	9.980	1803	7.1	6.6	0.5	0.6	0.4	1.2
DESI	−61.074	16.304	2013.098	2018.839	5.741	1710	0.2	0.1	−0.9	0.5	0.5	1.4
DHS0	−61.765	16.289	2011.143	2014.998	3.855	1086	−1.5	1.5	−17.0	1.4	1.5	6.5
DOR1	−74.663	5.454	2006.133	2018.839	12.706	2518	−12.6	5.4	0.7	0.3	0.3	1.1
DSD0	−61.066	16.312	2011.611	2014.998	3.387	1093	−0.6	0.8	−1.4	0.6	0.7	2.5
ELEN	−89.868	16.916	2002.004	2016.131	14.127	3679	−16.7	−2.1	1.5	0.3	0.3	1.1

Table A1. *Cont.*

	Long.	Lat.	Start*	End	Observations		Site Velocity (CARIB18) (mm/year) **			Velocity Uncertainty (mm/year) **		
GPS	(Degree)		(Decimal Year)		(Years)	(Days)	EW	NS	UD	EW	NS	UD
ELVI	−85.446	10.395	2007.332	2018.702	11.370	2254	−6.7	10.2	4.2	0.7	0.7	1.8
EMPR	−66.530	18.477	2015.499	2018.527	3.028	737	−0.8	0.2	−3.4	0.7	0.6	2.3
EPZA	−85.568	10.141	2009.503	2018.839	9.336	2752	−8.7	6.2	−4.4	1.4	1.3	1.2
ETCG	−84.106	9.999	2003.247	2018.839	15.592	4725	−1.3	11.4	−0.5	0.4	0.4	1.1
EXU0	−75.873	23.564	2007.494	2015.567	8.074	2432	−15.6	−4.3	−1.2	0.3	0.3	1.0
FFE0	−61.512	16.217	2003.072	2012.967	9.895	1653	1.1	2.9	1.7	0.6	0.7	1.4
FNA0	−61.582	15.875	2004.909	2012.564	7.655	1619	0.0	−0.2	−0.8	0.7	0.7	2.3
FOR1	−61.683	10.171	2007.034	2011.327	4.293	326	−15.5	−4.1	−5.3	0.5	0.7	2.3
FQNE	−73.735	5.467	2007.688	2018.839	11.151	1805	−13.1	4.9	0.7	0.2	0.4	0.8
FSDC	−61.147	14.735	2003.086	2014.787	11.702	2669	0.4	0.2	−2.7	0.5	0.5	2.0
GAL1	−60.995	10.147	2007.036	2011.327	4.290	354	−12.1	−8.7	−0.5	0.9	0.8	2.3
GARA	−73.360	5.081	2012.936	2018.839	5.903	1233	−17.0	1.6	0.7	0.4	0.4	1.4
GCEA	−81.378	19.293	2013.224	2018.839	5.615	1879	−16.5	−4.7	−1.6	0.5	0.6	1.5
GCFS	−81.184	19.313	2013.224	2018.839	5.615	1796	−16.2	−4.0	−0.2	0.5	0.5	1.3
GCGT	−81.379	19.293	2005.440	2011.896	6.456	2048	−16.6	−4.1	−1.4	0.4	0.4	1.3
GERD	−62.194	16.795	2004.233	2018.398	14.166	4146	0.5	7.0	5.5	0.5	0.5	1.4
GOSI	−61.481	16.206	2013.082	2018.839	5.758	1853	0.6	0.4	−0.6	0.5	0.5	1.6
GRA3	−61.128	10.586	2007.036	2011.327	4.290	319	−2.0	−2.6	−1.8	0.5	0.6	2.6
GRE0	−61.640	12.222	2007.488	2016.238	8.750	2921	0.7	−0.1	−1.0	0.4	0.3	1.2
GRZA	−85.636	9.916	2006.338	2018.839	12.501	3668	5.1	20.1	−7.7	0.5	0.9	1.3
GTK0	−71.145	21.433	2007.491	2014.798	7.307	2158	−15.7	−5.4	−1.7	0.3	0.3	1.0
GUAT	−90.520	14.590	2002.001	2018.839	16.838	5570	−6.5	−0.3	−0.3	0.3	0.2	0.8
HATI	−85.710	10.292	2006.456	2017.952	11.496	3150	−1.4	15.8	−3.0	0.5	0.6	1.2
HERH	−86.831	12.609	2010.196	2016.471	6.275	1813	−7.7	2.0	−3.3	0.7	1.0	2.5
HOYN	−86.828	12.599	2010.196	2015.381	5.185	1821	−8.6	1.4	−1.4	0.6	0.7	2.3
HUA2	−85.352	10.018	2002.732	2018.426	15.693	4643	1.7	18.4	−3.4	0.6	0.5	0.9
HUPR	−65.839	18.149	2015.499	2018.839	3.340	854	−2.2	−0.1	−5.2	0.9	1.0	2.8
IBAG	−75.215	4.428	2006.136	2018.839	12.704	2161	−14.6	5.2	1.5	0.3	0.4	1.1
ICAM	−90.527	19.853	2009.005	2018.801	9.796	2692	−16.3	−2.5	−2.6	0.3	0.3	1.0
IGN1	−79.536	8.985	2008.578	2018.579	10.001	2904	3.9	5.0	0.8	0.4	0.4	1.1
IGPR	−66.107	17.965	2015.825	2018.839	3.014	860	−1.2	−1.0	−4.2	1.0	0.7	2.2
IND1	−85.502	9.865	2002.565	2018.839	16.274	4949	2.3	23.9	−9.8	0.5	0.6	1.0
ISCO	−87.056	5.544	2011.384	2018.839	7.455	2310	34.4	69.6	−0.7	0.5	0.5	1.6
JACO	−84.659	9.662	2011.154	2014.790	3.636	1312	−4.4	−7.4	11.5	1.0	1.7	3.1
JCFI	−86.828	12.684	2010.760	2017.758	6.998	1730	−5.3	0.7	1.2	0.5	0.6	1.7
JME2	−72.538	18.235	2013.470	2018.839	5.369	1291	−2.9	−3.1	−1.1	0.3	0.4	1.7
JMEL	−72.536	18.235	2010.201	2013.459	3.258	923	−5.1	−1.2	−1.8	0.8	0.7	2.5
KYW5	−81.653	24.582	2002.001	2016.591	14.590	5109	−15.4	−3.9	−0.6	0.2	0.2	0.7
KYW6	−81.653	24.582	2002.001	2016.591	14.590	4407	−15.8	−4.2	−0.5	0.2	0.2	1.0
LAFE	−84.960	9.807	2009.517	2018.839	9.322	3261	−3.1	11.4	0.3	1.0	1.4	1.9
LBO_	−74.082	4.638	2007.526	2018.330	10.804	2335	−18.3	5.6	−36.7	0.3	0.3	1.4
LCAY	−73.754	18.188	2010.212	2016.479	6.267	1264	−1.3	0.5	−3.2	0.6	0.5	2.0
LCSB	−80.082	19.668	2013.216	2018.839	5.624	1752	−15.0	−4.4	−1.9	0.4	0.5	1.3
LEME	−86.909	12.427	2009.908	2018.839	8.931	1989	−10.4	7.1	0.7	0.5	0.4	1.2
LEPA	−85.031	9.945	2006.316	2018.839	12.523	4331	−0.4	13.1	2.8	0.8	0.7	1.4
LMMF	−60.996	14.595	2008.509	2018.839	10.330	2271	0.9	0.0	−1.5	0.4	0.3	1.2
LMNL	−85.053	10.268	2007.340	2018.839	11.499	3175	−1.0	14.1	2.4	0.6	0.6	1.2
LORI	−61.052	14.825	2013.103	2018.839	5.736	1858	1.0	−0.1	−0.9	0.5	0.4	1.4
LSAM	−74.220	11.251	2008.622	2012.731	4.110	186	−4.0	6.9	−1.9	2.5	1.9	7.1
LVEG	−70.531	19.223	2005.752	2018.839	13.087	4259	−8.3	−4.6	−1.0	0.2	0.2	1.0
MA00	−71.624	10.674	2002.001	2014.763	12.761	3682	−4.2	2.1	−1.0	0.4	0.3	1.2
MAG2	−61.306	15.890	2013.090	2018.839	5.750	1093	0.8	0.0	−1.8	0.5	0.5	1.5
MANA	−86.249	12.149	2002.001	2018.839	16.838	5567	−4.8	4.5	−0.7	0.3	0.3	0.8
MAYZ	−67.159	18.218	2010.103	2017.717	7.614	2069	−0.4	0.0	−2.4	0.4	0.4	1.2
MEDE	−75.579	6.199	2005.862	2018.839	12.978	3103	−11.3	5.6	0.9	0.4	0.4	1.0
MERI	−89.620	20.980	2003.165	2018.839	15.674	4416	−16.2	−2.8	−1.4	0.2	0.2	0.7
MIPR	−66.527	17.886	2008.359	2017.714	9.355	2513	−0.2	0.3	−0.2	0.3	0.3	1.0
MMD1	−89.663	20.932	2008.320	2018.839	10.519	3675	−15.8	−2.8	−0.9	0.3	0.3	0.9
MOPR	−67.931	18.077	2008.824	2016.498	7.674	1494	−0.8	−1.0	1.4	0.3	0.3	1.0
MRTN	−60.858	14.471	2013.103	2018.839	5.736	1611	0.9	0.8	−2.6	0.5	0.5	1.7
MTHN	−81.049	24.726	2002.935	2006.209	3.274	921	−14.5	−4.0	−0.3	0.5	0.5	1.8

Table A1. *Cont.*

	Long.	Lat.	Start*	End	Observations		Site Velocity (CARIB18) (mm/year) **			Velocity Uncertainty (mm/year) **		
GPS	**(Degree)**		**(Decimal Year)**		**(Years)**	**(Days)**	**EW**	**NS**	**UD**	**EW**	**NS**	**UD**
MTP1	−92.368	14.791	2008.320	2018.839	10.519	3275	−15.1	1.8	−2.0	0.6	0.6	1.1
NAR1	−90.810	17.227	2011.140	2015.836	4.695	934	−17.6	−2.5	−0.5	0.7	0.7	2.2
NWBL	−62.203	16.820	2012.326	2018.398	6.073	2127	−0.9	6.9	4.0	0.5	0.5	1.4
OLVN	−62.228	16.750	2004.181	2018.398	14.218	4453	−0.6	2.6	2.2	0.9	0.5	2.0
P780	−66.579	18.075	2008.405	2018.839	10.434	3732	−0.8	0.4	−1.1	0.3	0.3	1.1
PAM2	−72.648	7.384	2012.830	2018.839	6.010	1395	−11.8	3.5	0.2	0.4	0.5	1.6
PDPR	−66.023	18.020	2015.825	2018.839	3.014	460	−2.4	−0.1	−7.4	1.1	0.9	4.2
PER2	−75.690	4.793	2006.029	2017.739	11.710	2733	−13.7	6.1	1.6	0.4	0.3	1.1
PMB1	−55.145	5.828	2005.999	2018.839	12.841	4217	−19.9	−5.1	−3.4	0.3	0.3	1.2
PMEC	−80.329	8.488	2015.447	2018.596	3.149	766	5.9	3.9	−2.1	0.8	0.9	2.7
PMPA	−79.561	8.955	2006.494	2009.823	3.329	861	10.5	3.5	−5.7	2.1	0.7	2.3
PNE2	−85.829	10.195	2009.531	2018.839	9.309	2730	−5.0	5.7	−2.9	0.9	1.0	1.5
PNEG	−85.829	10.196	2005.210	2009.599	4.389	1464	0.4	15.3	−5.0	0.5	0.6	1.7
POLS	−86.813	12.649	2010.190	2017.339	7.149	1356	−5.5	2.4	−1.5	0.5	0.4	1.5
POPT	−89.410	16.325	2011.140	2014.804	3.663	642	−16.6	−4.5	−0.2	1.1	0.8	2.4
PRAR	−66.647	18.450	2010.092	2018.839	8.748	2983	−0.9	0.6	−0.4	0.3	0.4	1.3
PRFJ	−65.651	18.326	2012.909	2018.839	5.930	2043	−0.7	1.0	−1.0	0.4	0.4	1.4
PRGY	−66.814	18.051	2010.270	2018.839	8.570	2873	−0.4	−0.3	−3.4	0.4	0.4	1.5
PRHL	−66.154	18.380	2010.349	2018.839	8.490	2919	−1.4	−0.1	−1.4	0.3	0.4	1.5
PRJC	−67.000	18.342	2010.267	2018.839	8.572	2931	−1.3	0.2	−2.2	0.4	0.4	1.5
PRLP	−65.868	18.195	2010.418	2018.839	8.422	2853	−0.4	0.9	−1.1	0.4	0.4	1.5
PRLT	−67.189	18.060	2010.418	2018.839	8.422	2925	−1.3	1.4	−0.9	0.3	0.4	1.3
PRMI	−67.045	17.970	2006.240	2018.839	12.600	4301	−1.0	−0.8	−0.2	0.2	0.3	0.9
PRN4	−66.369	18.079	2010.092	2018.839	8.748	2992	−1.3	−0.1	0.0	0.4	0.4	1.3
PROX	−89.667	21.303	2011.907	2015.083	3.176	1032	−15.7	−4.1	−1.5	0.6	0.5	1.9
PRSN	−67.145	18.217	2015.825	2018.839	3.014	948	−1.5	−1.1	−0.2	0.8	0.7	3.4
PUAR	−82.830	8.310	2014.311	2018.333	4.022	872	12.5	15.8	2.0	0.6	1.1	2.8
PUJE	−85.272	10.114	2002.763	2018.839	16.077	4404	1.9	17.9	−1.1	0.5	0.4	0.9
PUMO	−84.967	10.065	2007.316	2018.839	11.524	3757	−0.9	12.2	0.8	0.6	0.7	1.3
PUR5	−67.067	18.463	2002.001	2016.591	14.590	5034	−1.1	0.3	−0.3	0.2	0.3	1.0
PUR6	−67.067	18.463	2007.636	2016.591	8.956	2991	−1.3	0.8	0.2	0.3	0.3	1.2
QSEC	−85.357	9.840	2006.324	2018.839	12.515	3971	−0.7	18.3	−6.2	0.7	0.6	1.1
QUEN	−86.852	12.592	2010.204	2018.694	8.490	1711	−8.0	6.3	−2.1	0.5	0.6	1.6
QUIB	−76.657	5.700	2008.104	2018.738	10.634	1718	−12.4	6.6	0.0	0.4	0.4	1.4
RCHY	−62.153	16.704	2012.326	2018.398	6.073	1855	1.8	−1.9	6.2	0.5	0.4	1.6
RDF2	−70.680	19.452	2015.436	2018.839	3.403	1163	−11.9	−2.7	−0.3	2.0	0.6	2.2
RDLT	−69.547	19.307	2015.275	2018.839	3.565	1163	−12.6	−1.9	−1.8	0.5	1.0	2.5
RDON	−62.346	16.934	2012.397	2018.839	6.442	1832	0.4	0.1	−0.4	0.5	0.4	1.2
RDSD	−69.911	18.461	2007.682	2018.398	10.716	2835	−1.9	−3.6	0.5	0.3	0.3	1.5
RIOH	−72.870	11.513	2005.815	2014.721	8.906	1390	−2.5	4.6	1.7	0.2	0.3	1.0
ROA0	−86.527	16.318	2007.359	2018.826	11.466	3502	1.4	3.3	−1.4	0.4	0.4	1.0
SABY	−91.187	18.967	2012.685	2015.858	3.173	662	−16.0	−3.3	10.2	0.7	0.7	2.6
SAJU	−85.711	10.067	2008.241	2018.839	10.598	3720	1.6	14.9	−6.4	0.6	0.9	1.3
SAMA	−74.187	11.225	2006.341	2018.839	12.498	3403	−2.9	4.9	−3.9	0.4	0.4	1.5
SAN0	−81.716	12.580	2007.937	2017.990	10.053	3419	1.2	0.5	−0.1	0.3	0.3	0.9
SCUB	−75.762	20.012	2002.001	2018.817	16.816	3600	−13.7	−4.5	−0.8	0.3	0.3	1.0
SINC	−75.388	9.316	2013.073	2018.839	5.766	1440	−2.6	2.2	0.3	0.6	0.5	1.7
SMRT	−63.109	18.042	2007.392	2016.690	9.298	3348	−0.7	0.6	−0.4	0.4	0.3	1.1
SNJE	−89.601	13.868	2007.220	2017.999	10.779	3333	−5.2	1.6	−2.4	0.3	0.4	0.8
SNSN	−75.308	5.715	2013.925	2018.839	4.915	1028	−11.9	5.3	−0.5	0.6	0.6	2.2
SPED	−69.306	18.461	2005.752	2018.839	13.087	4312	−2.4	−3.3	−0.7	0.2	0.2	0.9
SRCS	−55.569	5.846	2015.066	2018.836	3.770	558	−21.7	−2.4	−8.5	0.6	0.7	1.9
SRNW	−56.992	5.945	2006.026	2015.669	9.643	3131	−20.0	−5.2	−1.3	0.3	0.3	1.4
SROD	−71.341	19.475	2005.752	2018.839	13.087	4353	−9.4	−5.3	−0.7	0.3	0.3	1.0
SRZN	−55.203	5.456	2006.095	2018.839	12.745	3445	−20.6	−5.1	−0.4	0.3	0.3	1.2
SSIA	−89.117	13.697	2002.001	2018.335	16.334	4112	−3.6	2.1	0.8	0.3	0.5	0.8
STVI	−64.974	18.340	2008.824	2018.836	10.012	3018	−0.4	0.1	−1.2	0.4	0.4	1.1
SVGB	−61.250	13.275	2011.003	2018.448	7.444	2384	−0.1	−1.3	−0.4	0.7	0.5	1.9
TAXI	−90.465	14.035	2011.140	2015.390	4.249	1006	−11.9	3.3	−1.1	0.9	0.6	2.5
TECF	−86.838	12.603	2010.771	2017.541	6.771	2113	−9.3	4.1	−2.1	0.6	0.6	1.6

Table A1. *Cont.*

	Long.	Lat.	Start*	End	Observations		Site Velocity (CARIB18) (mm/year) **			Velocity Uncertainty (mm/year) **		
GPS	(Degree)		(Decimal Year)		(Years)	(Days)	EW	NS	UD	EW	NS	UD
TEG2	−87.206	14.090	2002.001	2018.204	16.203	2306	−1.7	2.7	−0.3	0.3	0.3	1.3
TELN	−86.835	12.606	2009.982	2017.235	7.253	2215	−8.2	5.4	−2.9	0.6	0.8	1.3
TGDR	−71.092	18.208	2015.518	2018.839	3.321	1186	−0.2	0.2	−0.1	0.8	0.7	1.8
TNPJ	−93.219	15.705	2014.886	2018.749	3.863	1123	−15.7	−0.7	−10.6	0.8	0.9	4.4
TRIL	−61.033	14.539	2013.098	2018.839	5.741	1806	0.8	0.1	−2.1	0.5	0.5	1.6
TRNT	−62.163	16.764	2004.252	2018.398	14.147	4211	1.4	9.5	10.6	0.4	0.5	1.5
TTSF	−61.466	10.277	2015.357	2018.839	3.483	1253	−15.9	−5.6	−5.6	0.6	0.6	1.7
TTUW	−61.399	10.640	2014.037	2018.839	4.802	1315	−1.0	−2.2	−1.7	0.5	0.7	2.2
TUNA	−73.364	5.531	2005.821	2018.839	13.019	3742	−14.4	3.2	−0.3	0.2	0.2	0.7
UCRI	−84.052	9.936	2015.529	2018.839	3.310	817	−12.7	5.1	−2.3	1.7	2.4	2.3
UNPM	−86.868	20.869	2007.603	2018.839	11.236	3942	−16.2	−3.6	−0.9	0.3	0.2	0.9
VAL2	−73.252	10.474	2006.018	2017.144	11.127	2622	−4.8	4.2	0.4	0.3	0.3	1.2
VDPR	−73.248	10.436	2015.003	2018.387	3.384	933	−4.7	3.6	−15.1	0.6	0.6	3.8
VERA	−84.869	10.854	2009.588	2018.839	9.251	3187	−1.9	1.4	0.3	0.6	0.8	1.2
VIKH	−64.798	17.716	2006.650	2017.547	10.897	3309	1.2	−0.4	−2.0	0.3	0.4	1.1
VIL2	−92.931	17.990	2003.165	2018.801	15.636	2409	−16.8	−1.3	−1.7	0.3	0.3	1.1
VITH	−64.969	18.343	2006.631	2018.839	12.208	3824	−0.9	0.3	−0.8	0.3	0.4	0.9
VIVI	−73.584	4.075	2005.802	2018.839	13.038	3075	−20.2	−0.1	−0.9	0.3	0.4	0.9
VLCN	−82.639	8.785	2011.379	2016.753	5.374	1916	7.1	9.0	0.8	0.6	0.6	2.2
VMAG	−74.847	9.287	2012.334	2018.650	6.316	1934	−5.2	3.9	3.3	0.6	0.4	1.4
VMIG	−88.305	13.396	2007.491	2018.004	10.513	3653	−7.9	4.2	0.8	0.6	0.6	1.4
VORA	−76.722	7.818	2015.003	2018.650	3.647	801	2.7	3.8	−17.4	1.0	1.1	3.8
VPOL	−74.861	10.794	2015.003	2018.650	3.647	1269	−4.7	5.1	−3.0	0.6	0.5	2.2
VRAI	−83.191	9.925	2012.802	2018.590	5.788	1858	3.6	5.0	−6.4	0.5	0.5	2.2
YOPA	−72.389	5.322	2005.895	2015.266	9.372	853	−19.4	0.4	1.2	0.3	0.3	0.9
ZARZ	−76.068	4.397	2012.936	2018.839	5.903	1404	−13.7	4.6	0.5	0.4	0.5	1.6
ZSU1	−65.993	18.431	2003.198	2011.797	8.600	2921	−0.8	0.4	1.3	0.3	0.4	1.5
ZSU4	−65.993	18.431	2012.906	2018.839	5.933	2040	−1.0	0.9	−1.5	0.4	0.5	1.7

* JPL had not released its IGS14 orbit and clock data products for epochs before 2002 at the time we processed data for this study (December 2018). For this reason, GPS observations before 2002 were not processed.
** The velocity and uncertainty were estimated using the MIDAS method [53].

References

1. Dixon, T.H.; Gonzalez, G.; Lichten, S.M.; Katsigris, E. First epoch geodetic measurements with the Global Positioning System across the northern Caribbean plate boundary zone. *J. Geophys. Res.* **1991**, *96*, 2397–2415. [CrossRef]
2. Dixon, T.H. GPS Measurement of relative motion of the Cocos and Caribbean plates and strain accumulation across the Middle America Trench. *Geophys. Res. Lett.* **1993**, *20*, 2167–2170. [CrossRef]
3. Freymueller, J.T.; Kellogg, J.N.; Vega, V. Plate motions in the North Andean Region. *J. Geophys. Res.* **1993**, *98*, 21853–21863. [CrossRef]
4. DeMets, C.; Jansma, P.E.; Mattioli, G.S.; Dixon, T.H.; Farina, F.; Bilham, R.; Calais, E.; Mann, P. GPS geodetic constraints on Caribbean-North America plate motion. *Geophys. Res. Lett.* **2000**, *27*, 437–440. [CrossRef]
5. Burke, K.; Grippi, J.; Şengör, A.C. Neogene structures in Jamaica and the tectonic style of the northern Caribbean plate boundary zone. *J. Geol.* **1980**, *88*, 375–386. [CrossRef]
6. Mann, P.; Burke, K. Neotectonics of the Caribean. *Rev. Geophys. Space Sci.* **1984**, *22*, 309–362. [CrossRef]
7. Bird, P. An updated digital model of plate boundaries. *Geochem. Geophys. Geosyst.* **2003**, *4*, 1027. [CrossRef]
8. Benford, B.; DeMets, C.; Calais, E. GPS estimates of microplate motions, northern Caribbean: Evidence for a Hispaniola microplate and implications for earthquake hazard. *Geophys. J. Int.* **2012**, *191*, 481–490. [CrossRef]
9. Benford, B.; DeMets, C.; Tikoff, B.; Williams, P.; Brown, L.; Wiggins-Grandison, M. Seismic hazard along the southern boundary of the Gônave microplate: Block modelling of GPS velocities from Jamaica and nearby islands, northern Caribbean. *Geophys. J. Int.* **2012**, *190*, 59–74. [CrossRef]
10. Liu, H.; Wang, G. Relative motion between St. Croix and the Puerto Rico-Virgin Islands block derived from continuous GPS observations (1995–2014). *Int. J. Geophys.* **2015**, 915753. [CrossRef]

11. Weber, J.C.; Geirsson, H.; Latchman, J.L.; Shaw, K.; La Femina, P.; Wdowinski, S.; Higgins, M.; Churches, C.; Norabuena, E. Tectonic inversion in the Caribbean-South American plate boundary: GPS geodesy, seismology, and tectonics of the Mw 6.7 22 April 1997 Tobago earthquake. *Tectonics* **2015**, *34*, 1181–1194. [CrossRef]
12. Calais, E.; Symithe, S.; de Lépinay, B.M.; Prépetit, C. Plate boundary segmentation in the northeastern Caribbean from geodetic measurements and Neogene geological observations. *C. R. Geosci.* **2016**, *348*, 42–51. [CrossRef]
13. Pérez, O.J.; Wesnousky, S.G.; Rosa, R.; Márquez, J.; Uzcátegui, R.; Quintero, C.; Liberal, L.; Mora-Páez, H.; Szeliga, W. On the interaction of the North Andes plate with the Caribbean and South American plates in northwestern South America from GPS geodesy and seismic data. *Geophys. J. Int.* **2018**, *214*, 1986–2001. [CrossRef]
14. Herring, T.A.; Melbourne, T.I.; Murray, M.H.; Floyd, M.A.; Szeliga, W.M.; King, R.W.; Phillips, D.A.; Puskas, C.M.; Santillan, M.; Wang, L. Plate Boundary Observatory and Related Networks: GPS Data Analysis Methods and Geodetic Products. *Rev. Geophys.* **2016**, *54*, 759–808. [CrossRef]
15. Blewitt, G.; Hammond, W.C.; Kreemer, C. Harnessing the GPS data explosion for interdisciplinary science. *EOS* **2018**, 99. [CrossRef]
16. Yang, L.; Wang, G.; Bao, Y.; Kearns, T.J.; Yu, J. Comparisons of Ground-Based and Building-Based CORS: A Case Study in the Puerto Rico and Virgin Islands Region. *J. Surv. Eng.* **2015**, *142*, 05015006. [CrossRef]
17. Braun, J.J.; Mattioli, G.S.; Calais, E.; Carlson, D.; Dixon, T.; Jackson, M.; Kursinski, R.; Mora-Paez, H.; Miller, M.M.; Pandya, R.; et al. Multi-Disciplinary Natural Hazards Research Initiative Begins Across the Caribbean Basin. *EOS Trans. Am. Geophys. Union* **2012**, *93*, 89–90. [CrossRef]
18. Rebischung, P.; Griffiths, J.; Ray, J.; Schmid, R.; Collilieux, X.; Garayt, B. IGS08: The IGS realization of ITRF2008. *GPS Solut.* **2012**, *16*, 483–494. [CrossRef]
19. Altamimi, Z.; Rebischung, P.; Métivier, L.; Collilieux, X. ITRF2014: A new release of the International Terrestrial Reference Frame modeling nonlinear station motions. *J. Geophys. Res.* **2016**, *121*, 6109–6131. [CrossRef]
20. Rebischung, P.; Altamimi, Z.; Ray, J.; Garayt, B. The IGS contribution to ITRF2014. *J. Geod.* **2016**, *90*, 611–630. [CrossRef]
21. Geng, J.; Meng, X.; Dodson, A.H.; Teferle, F.N. Integer ambiguity resolution in precise point positioning: Method comparison. *J. Geod.* **2010**, *84*, 569–581. [CrossRef]
22. Li, X.; Zhan, X.; Ge, M. Regional reference network augmented precise point positioning for instantaneous ambiguity resolution. *J. Geod.* **2011**, *85*, 151–158. [CrossRef]
23. Wang, G. GPS landslide monitoring: Single base vs. network solutions: A case study based on the Puerto Rico and Virgin Islands permanent GPS network. *J. Geod. Sci.* **2011**, *1*, 191–203. [CrossRef]
24. Wang, G. Millimeter-accuracy GPS landslide monitoring using precise point positioning with single receiver phase ambiguity resolution: A case study in Puerto Rico. *J. Geod. Sci.* **2013**, *3*, 22–31. [CrossRef]
25. Zumberge, J.; Heflin, M.; Jefferson, D.; Watkins, M.; Webb, F. Precise point positioning for the efficient and robust analysis of GPS data from large networks. *J. Geophys. Res.* **1997**, *102*, 5005–5017. [CrossRef]
26. Wang, G.; Bao, Y.; Cuddus, Y.; Jia, X.; Serna, J.; Jing, Q. A methodology to derive precise landslide displacement time series from continuous GPS observations in tectonically active and cold regions: A case study in Alaska. *Nat. Hazards* **2015**, *77*, 1939–1961. [CrossRef]
27. Bao, Y.; Guo, W.; Wang, G.; Gan, W.; Zhang, M.; Shen, J.S. Millimeter-accuracy structural deformation monitoring using stand-alone GPS: Case study in Beijing, China. *J. Surv. Eng.* **2017**, *144*, 05017007. [CrossRef]
28. Bertiger, W.; Desai, S.D.; Haines, B.; Harvey, N.; Moore, A.W.; Owen, S.; Weiss, J.P. Single receiver phase ambiguity resolution with GPS data. *J. Geod.* **2010**, *84*, 327–337. [CrossRef]
29. Wang, G.; Bao, Y.; Gan, W.; Geng, J.; Xiao, G.; Shen, J.S. NChina16: A stable geodetic reference frame for geological hazard studies in North China. *J. Geodyn.* **2018**, *115*, 10–22. [CrossRef]
30. Firuzabadi, D.; King, R.W. GPS precision as a function of session duration and reference frame using multi-point software. *GPS Solut.* **2012**, *16*, 191–196. [CrossRef]
31. Wang, G.; Soler, T. Measuring land subsidence using GPS: Ellipsoid height vs. orthometric height. *J. Surv. Eng.* **2014**, *141*, 05014004. [CrossRef]
32. Booker, D.; Clarke, P.J.; Lavallee, D.A. Secular changes in Earth's shape and surface mass loading derived from combinations of reprocessed global GPS networks. *J. Geod.* **2014**, *88*, 839–855. [CrossRef]

33. Blewitt, G.; Kreemer, C.; Hammond, W.C.; Goldfarb, J.M. Terrestrial reference frame NA12 for crustal deformation studies in North America. *J. Geodyn.* **2013**, *72*, 11–24. [CrossRef]
34. Pearson, C.; Snay, R. Introducing HTDP 3.1 to transform coordinates across time and spatial reference frames. *GPS Solut.* **2013**, *17*, 1–15. [CrossRef]
35. Wang, G.; Kearns, T.J.; Yu, J.; Saenz, G. A stable reference frame for landslide monitoring using GPS in the Puerto Rico and Virgin Islands region. *Landslides* **2014**, *11*, 119–129. [CrossRef]
36. Soler, T.; Marshall, J. Rigorous transformation of variance-covariance matrices of GPS-derived coordinates and velocities. *GPS Solut.* **2002**, *6*, 76–90. [CrossRef]
37. Soler, T.; Snay, R.A. Transforming positions and velocities between the International Terrestrial Reference Frame of 2000 and North American Datum of 1983. *J. Surv. Eng.* **2004**, *130*, 49–55. [CrossRef]
38. Sella, G.F.; Dixon, T.H.; Mao, A. REVEL: A model for recent plate velocities from space geodesy. *J. Geophys. Res.* **2002**, *107*, B4. [CrossRef]
39. Blewitt, G. Self-consistency in reference frames, geocenter definition, and surface loading of the solid Earth. *J. Geophys. Res.* **2003**, *108*, 210. [CrossRef]
40. Yu, J.; Wang, G. GPS-derived ground deformation (2005–2014) within the Gulf of Mexico region referred to a stable Gulf of Mexico reference frame. Nat. Hazards. *Earth Syst. Sci.* **2016**, *16*, 1583–1602. [CrossRef]
41. Wang, G.; Turco, M.; Soler, T.; Kearns, T.; Welch, J. Comparisons of OPUS and PPP solutions for subsidence monitoring in the greater Houston area. *J. Surv. Eng.* **2017**, *143*, 05017005. [CrossRef]
42. Kearns, T.J.; Wang, G.; Turco, M.; Welch, J.; Tsibanos, V.; Liu, H. Houston16: A stable geodetic reference frame for subsidence and faulting study in the Houston metropolitan area, Texas, U.S. *Geod. Geodyn.* **2018**. [CrossRef]
43. DeMets, C.; Mattioli, G.; Jansma, P.; Rogers, R.D.; Tenorio, C.; Turner, H.L.; Mann, P. Present motion and deformation of the Caribbean plate: Constraints from new GPS geodetic measurements from Honduras and Nicaragua. *Geol. Soc. Am.* **2007**, *428*, 21.
44. DeMets, C.; Gordon, R.G.; Argus, D.F. Geologically current plate motions. *Geophys. J. Int.* **2010**, *181*, 1–80. [CrossRef]
45. Symithe, S.; Calais, E.; Chabalier, J.B.; Robertson, R.; Higgins, M. Current block motions and strain accumulation on active faults in the Caribbean. *J. Geophys. Res. (Solid Earth)* **2015**, *120*, 3748–3774. [CrossRef]
46. Yang, L.; Wang, G.; Huérfano, V.; Hillebrandt-Andrade, C.G.; Martínez-Cruzado, J.A.; Liu, H. GPS geodetic infrastructure for natural hazards study in the Puerto Rico and Virgin Islands region. *Nat. Hazards* **2016**, *83*, 641–665. [CrossRef]
47. Yu, J.; Wang, G. Introduction to the GNSS Geodetic Infrastructure in the Gulf of Mexico Region. *Surv. Rev.* **2017**, *352*, 51–65. [CrossRef]
48. Wang, G.; Yu, J.; Ortega, J.; Saenz, G.; Burrough, T.; Neill, R. A stable reference frame for the study of ground deformation in the Houston metropolitan area, Texas. *J. Geod. Sci.* **2013**, *3*, 188–202. [CrossRef]
49. Argus, D.F.; Gordon, R.G.; DeMets, C. Geologically current motion of 56 plates relative to the no-net-rotation reference frame. *Geochem. Geophys. Geosyst.* **2011**, *12*. [CrossRef]
50. Huérfano, V.; von Hillebrandt-Andrade, C.; Báez-Sanchez, G. Microseismic activity reveals two stress regimes in southwestern Puerto Rico. *Geol. Soc. Am. Spec. Pap.* **2005**, *385*, 81–101.
51. Joyce, J.; McCann, W.R.; Lithgow, C. Onland active faulting in the Puerto Rico platelet. *EOS (Trans. Am. Geophys. Union)* **1987**, *68*, 1483.
52. Prentice, C.S.; Mann, P. Paleoseismic study of the South Lajas fault: First documentation of an onshore Holocene fault in Puerto Rico. *Geol. Soc. Am. Spec. Pap.* **2005**, *385*, 215–222.
53. Blewitt, G.; Kreemer, C.; Hammond, W.C.; Gazeaux, J. MIDAS robust trend estimator for accurate GPS station velocities without step detection. *J. Geophys. Res.* **2016**, *121*, 2054–2068. [CrossRef]
54. Dixon, T.H.; Farina, F.; DeMets, C.; Jansma, P.; Mann, P.; Calais, E. Relative motion between the Caribbean and North American plates and related boundary zone deformation from a decade of GPS observations. *J. Geophys. Res.* **1998**, *103*, 15157–15182. [CrossRef]
55. Jansma, P.E.; Mattioli, G.S.; Lopez, A.; DeMets, C.; Dixon, T.H.; Mann, P.; Calais, E. Neotectonics of Puerto Rico and the Virgin Islands, northeastern Caribbean, from GPS geodesy. *Tectonics* **2000**, *19*, 1021–1037. [CrossRef]
56. Jansma, P.E.; Mattioli, G.S.; Mann, P. GPS results from Puerto Rico and the Virgin Islands: Constraints on tectonic setting and rates of active faulting. *Geol. Soc. Am. Spec. Pap.* **2005**, *385*, 13–30.

57. Mann, P.; Calais, E.; Ruegg, J.C.; DeMets, C.; Jansma, P.E.; Mattioli, G.S. Oblique collision in the northeastern Caribbean from GPS measurements and geological observations. *Tectonics* **2002**, *21*, 71726. [CrossRef]
58. Ten Brink, U.; López-Venegas, A.M. Plate interactions in the NE Caribbean subduction zone from continuous GPS observations. *Geophys. Res. Lett.* **2012**, *39*, 10304. [CrossRef]
59. Freymueller, J.T.; Woodard, H.; Cohen, S.C.; Cross, R.; Elliott, J.; Larsen, C.F.; Hreinsdottir, S.; Zweck, C. Active deformation processes in Alaska, based on 15 years of GPS measurements. In *Active Tectonics and Seismic Potential of Alaska*; Geophys. Monogr. Ser.; AGU: Washington, DC, USA, 2008; Volume 179, pp. 1–42.
60. Suito, H.; Freymueller, J.T. A viscoelastic and afterslip postseismic deformation model for the 1964 Alaska earthquake. *J. Geophys. Res.* **2009**, *114*, B11404. [CrossRef]
61. Feng, L.; Newman, A.V.; Protti, M.; Gonzalez, V.; Jiang, Y.; Dixon, T.H. Active deformation near the Nicoya Peninsula, northwestern Costa Rica, between 1996 and 2010: Interseismic megathrust coupling. *J. Geophys. Res.* **2012**, *117*, B06407. [CrossRef]
62. Jiang, Y.; Wdowinski, S.; Dixon, T.H.; Hackl, M.; Protti, M.; Gonzalez, V. Slow slip events in Costa Rica detected by continuous GPS observations, 2002–2011. Geochem. *Geophys. Geosyst.* **2012**, *13*, Q04006. [CrossRef]
63. Protti, M.; González, V.; Newman, A.V.; Dixon, T.H.; Schwartz, S.Y.; Marshall, J.S.; Feng, L.; Walter, J.I.; Malservisi, R.; Owen, S.E. Nicoya earthquake rupture anticipated by geodetic measurement of the locked plate interface. *Nat. Geosci.* **2014**, *7*, 117–121. [CrossRef]
64. Dixon, T.H.; Jiang, Y.; Malservisi, R.; McCaffrey, R.; Voss, N.; Protti, M.; Gonzalez, V. Earthquake and tsunami forecasts: Relation of slow slip events to subsequent earthquake rupture. *Proc. Natl. Acad. Sci. USA* **2014**, *111*, 17039–17044. [CrossRef] [PubMed]
65. Tomblin, J.F. The Lesser Antilles and Aves Ridge. In *The Gulf of Mexico and the Caribbean*; Nairn, A.E.M., Stehli, F.G., Eds.; Springer: Boston, MA, USA, 1975; Chapter 11; pp. 467–500.
66. Vallance, J.W.; Schilling, S.P.; Matías, O.; Rose, W.I., Jr.; Howell, M.M. *Volcano Hazards at Fuego and Acatenango, Guatemala (No. 2001-431)*; US Geological Survey: Reston, VA, USA, 2001.
67. Mattioli, G.S.; Herd, R.A. Correlation of cyclic surface deformation recorded by GPS geodesy with surface magma flux at Soufrière Hills volcano, Montserrat. *Seismol. Res. Lett.* **2004**, *74*, 230.
68. Wadge, G.; Herd, R.; Ryan, G.; Calder, E.S.; Komorowski, J.C. Lava production at Soufrière Hills Volcano, Montserrat: 1995–2009. *Geophys. Res. Lett.* **2010**, *37*. [CrossRef]
69. Young, N.K.; Gottsmann, J. Shallow crustal mechanics from volumetric strain data: Insights from Soufriere Hills Volcano, Montserrat. *J. Geophys. Res. (Solid Earth)* **2015**, *120*, 1559–1571. [CrossRef]
70. Wadge, G.; Voight, B.; Sparks, R.S.J.; Cole, P.D.; Loughlin, S.C.; Robertson, R.E.A. An overview of the eruption of Soufrière Hills Volcano, Montserrat from 2000 to 2010. *Geol. Soc. Lond. Mem.* **2014**, *39*, 1–40. [CrossRef]
71. Elsworth, D.; Mattioli, G.; Taron, J.; Voight, B.; Herd, R. Implications of Magma Transfer Between Multiple Reservoirs on Eruption Cycling. *Science* **2008**, *322*, 246–248. [CrossRef]
72. Mattioli, G.S.; Herd, R.A.; Strutt, M.H.; Ryan, G.; Widiwijayanti, C.; Voight, B. Long term surface deformation of Soufrière Hills Volcano, Montserrat from GPS geodesy: Inferences from simple elastic inverse models. Geophys. *Res. Lett.* **2010**, *37*, L00E13. [CrossRef]
73. Rodgers, M.; Smith, P.J.; Mather, T.A.; Pyle, D.M. Quiescent-explosive transitions during dome-forming volcanic eruptions: Using seismicity to probe the volcanic processes leading to the 29 July 2008 vulcanian explosion of Soufrière Hills Volcano, Montserrat. *J. Geophys. Res. (Solid Earth)* **2016**, *121*, 8453–8471. [CrossRef]
74. Sheldrake, T.E.; Aspinall, W.P.; Odbert, H.M.; Wadge, G.; Sparks, R.S.J. Understanding causality and uncertainty in volcanic observations: An example of forecasting eruptive activity on Soufrière Hills Volcano, Montserrat. *J. Volcanol. Geotherm. Res.* **2017**, *341*, 287–300. [CrossRef]
75. Mattioli, G.S.; Dixon, T.H.; Farina, F.; Howell, E.S.; Jansma, P.E.; Smith, A.L. GPS measurement of surface deformation around Soufriere Hills volcano, Montserrat from October 1995 to July 1996. *Geophys. Res. Lett.* **1998**, *25*, 3417–3420. [CrossRef]